

*From the book, Aromaticity: Modern Computational Methods and Applications, edited by Israel Fernández, publishing 2021 by Elsevier, Inc. All rights reserved.*

## CHAPTER 5

# **Current density, current-density pathways and molecular aromaticity**

Maria Dimitrova and Dage Sundholm  
*Department of Chemistry, Faculty of Science,  
P.O. Box 55 (A.I. Virtanens plats 1),  
FIN-00014 University of Helsinki, Finland,  
E-mail: maria.dimitrova@helsinki.fi, dage.sundholm@helsinki.fi*

May 12, 2021

## Abstract

Current densities are induced in the electronic structure of molecules when they are exposed to external magnetic fields. Aromatic molecular rings sustain net diatropic ring currents, whereas the net ring current in antiaromatic molecular rings is paratropic and flows in the opposite, non-classical direction. We present computational methods and protocols to calculate, analyse and visualise magnetically induced current densities in molecules. Calculated ring-current strengths are used for quantifying the degree of aromaticity. The methods have been demonstrated by investigating ring-current strengths and the degree of aromaticity of aromatic, antiaromatic and non-aromatic six-membered hydrocarbon rings. Current-density pathways and ring-current strengths of aromatic and antiaromatic porphyrinoids and other polycyclic molecules have been studied. The aromaticity and current density of Möbius-twisted molecules has been investigated to find the dependence on the twist and the spatial deformation of the molecular ring. Current densities of fullerene, gaudiene and toroidal carbon nanotubes have also been studied.

## Keywords

Molecular aromaticity, magnetically induced current-density susceptibility, ring-current strength, current-density pathway, diatropic ring current, paratropic ring current, gauge-including atomic orbitals, nuclear magnetic shielding, magnetic shielding density, magnetic susceptibility

### 5.1 Magnetic fields in quantum mechanics

Magnetic fields interact with charged particles in motion and induce rotational motion (precession) of the particle. Electrostatic fields which are routinely studied with quantum chemistry methods are scalar fields, whereas magnetic fields are vector fields, rendering the interpretation of the electronic response to the magnetic field complicated as it requires specialised computational approaches. In the presence of an external magnetic field, the generalised momentum operator  $\mathbf{p}$  comprises the kinetic momentum operator  $\hat{\pi}$  and the magnetic vector potential  $\mathbf{A}$  of the magnetic field, which can be expressed as

$$\hat{\pi} = -i\hbar\nabla + e\mathbf{A}. \quad (5.1)$$

The vector potential defines the magnetic flux  $\mathbf{B}$  of the external magnetic field, which is commonly referred to as the magnetic-field strength. A uniform external magnetic field can be obtained as the curl of the vector potential,

$$\mathbf{B} = \nabla \times \mathbf{A}. \quad (5.2)$$

Many vector potentials define the same magnetic flux since adding the gradient of any differentiable scalar function (a gauge function) to the vector potential will give the same magnetic field.<sup>1</sup> Even though a uniform static magnetic field is independent of the chosen gauge function, the origin of the magnetic vector potential (gauge origin) must be defined. However, one has the freedom to choose a convenient gauge origin,  $\mathbf{O}$ , which relates the vector potential  $\mathbf{A}(\mathbf{r})$  to the magnetic flux  $\mathbf{B}$  of a constant uniform magnetic field as

$$\mathbf{A}(\mathbf{r}) = \frac{1}{2}\mathbf{B} \times \mathbf{r}_\mathbf{O}, \quad (5.3)$$

where  $\mathbf{r}_\mathbf{O} = \mathbf{r} - \mathbf{O}$  is the distance between the point  $\mathbf{r}$  and the gauge origin.

In quantum chemistry, the Coulomb gauge,  $\nabla \cdot \mathbf{A} = 0$ , is usually employed which reduces the number of terms in the Hamiltonian. The Hamiltonian describing the magnetic interaction consists of three terms, namely the field-free Hamiltonian  $\hat{H}^{(0)}$ , a term that depends linearly on the magnetic field  $\hat{H}^{(1)}$ , and a term with a quadratic dependence on  $\mathbf{A}$  denoted by  $\hat{H}^{(2)}$ ,

$$\hat{H} = \hat{H}^{(0)} + \hat{H}^{(1)}(\mathbf{A}) + \hat{H}^{(2)}(A^2). \quad (5.4)$$

Employing the definition of the magnetic flux in Eq. 5.3, the following terms are obtained:

$$\hat{H}^{(1)} = \frac{e}{2m_e}\mathbf{B} \cdot \hat{\mathbf{L}}, \quad (5.5)$$

$$\hat{H}^{(2)} = \frac{e^2}{8m_e} \left( B^2 r^2 - (\mathbf{B} \cdot \mathbf{r})^2 \right). \quad (5.6)$$

The term linear in  $\mathbf{B}$  describes the coupling between the external magnetic field and the

orbital angular momentum of the electron, whereas the quadratic term can be seen as the coupling between the induced magnetic moment of the electron and the external field. Since magnetic fields on Earth, both in nature and under laboratory conditions, are very weak compared to Coulomb interactions, the first-order dependence on  $\mathbf{B}$  in Eq. 5.5 can be studied using perturbation theory.

In the Hamiltonian of open-shell systems, a first-order term appears describing the interaction between the spin of the electron ( $\hat{\mathbf{S}}$ ) and the external magnetic field,

$$\hat{H}_S^{(1)} = \frac{e}{m_e} \mathbf{B} \cdot \hat{\mathbf{S}}. \quad (5.7)$$

However, in this chapter we do not account for interactions between the external magnetic field and the spin of the electron.

## 5.2 Current density

Current density  $\mathbf{j}(\mathbf{r})$  is a conserved property such that  $\nabla \cdot \mathbf{j}(\mathbf{r}) = 0$ , which is a direct consequence of charge conservation. In the general case, it was defined by Schrödinger as the continuity equation<sup>2</sup>

$$\mathbf{j}(\mathbf{r}) = -\frac{e}{2m_e} (\psi \hat{\mathbf{p}} \psi^* + \psi^* \hat{\mathbf{p}} \psi). \quad (5.8)$$

where  $\hat{\mathbf{p}}$  is the momentum operator,  $\psi$  is the wave function and  $\psi^*$  is its complex conjugate. Current densities are a subobservable that is in principle experimentally accessible and can be calculated as the expectation value of a quantum-mechanical operator.<sup>3</sup> However, at present there is no experimental method of directly probing the current density in a single molecule.

In the presence of an external magnetic field, the molecular wave function can be expressed as a sum of the zero-order field-free wave function,  $\Psi_0^{(0)}$ , and the first-order magnetically perturbed wave function,  $\Psi_0^{(1)}$ ,

$$\Psi_0 = \Psi_0^{(0)} + \Psi_0^{(1)}, \quad (5.9)$$

where the perturbed wave function can formally be written as a sum over the unperturbed wave functions of the excited states  $j$ ,



$$\Psi_0^{(1)} = \frac{e}{2m_e\hbar} \sum_{j \neq 0} |\Psi_j^{(0)}\rangle \frac{\langle \Psi_j^{(0)} | \hat{\mathbf{L}} \cdot \mathbf{B} | \Psi_0^{(0)} \rangle}{E_j^{(0)} - E_0^{(0)}}, \quad (5.10)$$

where  $E_0^{(0)}$  and  $E_j^{(0)}$  in the denominator of Eq. 5.10 are the energies of the ground and the  $j^{\text{th}}$  excited state. The terms in the numerator are the transition moments of the angular momentum operator between the ground state and the excited states. The angular momentum exerts the rotational motion around the gauge origin  $\mathbf{O}$  so that  $\hat{\mathbf{L}} = \mathbf{r}_\mathbf{O} \times \hat{\mathbf{p}}$ .

Inserting the wave function with the first-order perturbation correction from Eq. 5.9 into the expression in Eq. 5.8 leads to two terms that depend on the chosen gauge origin. The contributions to the current density that involve the ground-state wave function  $\Psi_0^{(0)}$  are called diamagnetic,  $\mathbf{J}_d^B$ , whereas the terms representing the sum over states are called paramagnetic,  $\mathbf{J}_p^B$ . This division is entirely arbitrary. The terms will change depending on the choice of the gauge origin. For example, the paramagnetic current density can be made to vanish completely.<sup>4,5</sup> Only the sum of the diamagnetic and paramagnetic has a physical meaning. The total current density is expressed as the sum of the diamagnetic and paramagnetic contributions as

$$\mathbf{J}^B = \mathbf{J}_d^B + \mathbf{J}_p^B \quad \begin{cases} \mathbf{J}_d^B &= -\frac{e^2}{2m_e} \mathbf{B} \times \mathbf{r}_\mathbf{O} (\Psi_0^{(0)})^2, \\ \mathbf{J}_p^B &= -i\hbar \frac{e^2}{m_e} \sum_{j \neq 0} (\Psi_j^{(1)} \nabla \Psi_0^{(0)} + \Psi_0^{(0)} \nabla \Psi_j^{(1)}). \end{cases} \quad (5.11)$$

The diamagnetic term can be interpreted as the Larmor precession of an electron in a magnetic field as in classical electrodynamics, while the paramagnetic term does not have a classical counterpart. Since the diamagnetic term depends only on the ground-state wave function, it means that all atoms and molecules exhibit a diamagnetic response.

Using the expression for the perturbed wave function in Eq. 5.10 for the paramagnetic term  $\mathbf{J}_p^B$  and employing the expressions for the magnetic field and the angular momentum in the chosen gauge origin in Eq. 5.3 leads to terms with two sets of integrals namely, transition moments with rotational symmetry involving the angular momentum operator,  $\langle \Psi_j^{(0)} | \hat{\mathbf{L}} | \Psi_0^{(0)} \rangle$ , and the terms proportional to  $\langle \Psi_j^{(0)} | \hat{\mathbf{p}} | \Psi_0^{(0)} \rangle$  which are, in turn, the transition moments involving the linear momentum operator. A thorough derivation of the formalism was recently presented by Berger, Monaco and Zanasi.<sup>1</sup>

### 5.3 Current-density susceptibility

The current density  $\mathbf{J}^B(\mathbf{r})$  induced by a weak magnetic field is a vector field can be expanded in a Taylor series with respect to the magnetic-field strength  $\mathbf{B}$ ,

$$\mathbf{J}^B(\mathbf{r}) = \mathbf{j}_0(\mathbf{r}) + \sum_{\beta \in \{x,y,z\}} \left. \frac{\partial \mathbf{J}^B(\mathbf{r})}{\partial B_\beta} \right|_{B_\beta=0} B_\beta + \mathcal{O}(B_\beta^2). \quad (5.12)$$

The zero-order term  $\mathbf{j}_0(\mathbf{r})$  vanishes for closed-shell molecules. The first-order terms are the first derivatives of the current density with respect to the  $x$ ,  $y$  and  $z$  components of the magnetic field. These derivatives are the current-density susceptibility of the molecule,<sup>6</sup>

$$\mathcal{J}_\alpha^{B_\beta}(\mathbf{r}) = \left. \frac{\partial J_\alpha^B(\mathbf{r})}{\partial B_\beta} \right|_{B_\beta=0}, \text{ where } \alpha, \beta \in \{x, y, z\}. \quad (5.13)$$

The current-density susceptibility is a rank-2 tensor describing the current-density flux in the  $\alpha$  direction when the magnetic field is applied in the  $\beta$  direction. Contracting the tensor with a particular magnetic field direction gives the first-order current-density vector field for the chosen orientation of the molecule with respect to the magnetic field.

### 5.4 Current-density vector field

The magnetically induced current density  $\mathbf{J}^B(\mathbf{r})$  is a unique fingerprint of the magnetic response of the electronic structure of a molecule. Since the first-order perturbed wave function  $\Psi_0^{(1)}$  can be written as a sum-over-state expression containing transition moments of operators with a given symmetry, it is obvious that orbital symmetry plays an important role for the topology of the current-density vector field.<sup>1,7-12</sup>

Saddle-stagnation points define closed surfaces (separatrices) that divide the current density into multiple domains.<sup>8,13</sup> A closed separatrix encases a vortex with a singular axis, around which the electrons move in a closed loop. Gomes showed that there is always a vortex which completely encloses the entire molecule.<sup>8</sup> Inside that global domain, many other vortices can exist, however, due to charge conservation, the separatrices may not cross.

The tropicity concept, originally introduced in fluid mechanics, can be employed to analyse the direction of the rotational motion in the current-density vortices with respect to the magnetic field.<sup>14</sup> In our convention, a vortex is labelled *diatropic* when the direction of the current density is clockwise when looking towards the negative direc-

tion of the magnetic field vector, which is in the classical direction according to Lenz's law.<sup>5,15</sup> When the electrons follow a pathway in the opposite direction, the current-density flux is termed *paratropic*. The tropicity is a property of the total current density carrying a physical meaning. It is not related to the similarly sounding diamagnetic and paramagnetic terms, which arise as a mathematical formality and depend on the gauge origin.

Diatropic current densities induce a secondary magnetic field which opposes the external magnetic field, while paratropic current densities give rise to a secondary magnetic field that strengthens the external field. In spite of the similarity of the names, diatropic and paratropic current densities cannot be mapped to the gauge-origin dependent diamagnetic and paramagnetic contributions to the current density. The diatropic current density generally originates from the diamagnetic current density expressed in Eq. 5.11, whereas the sum-over-states expression in Eq. 5.10 contains both linear- and angular-momentum transition moments which are responsible for diatropic and paratropic current densities, respectively.<sup>1,7</sup>

Furthermore, diamagnetism and paramagnetism denote the response of a material to an external magnetic field, which has no physical connection to the names of the terms derived in the perturbation-theory formalism.<sup>5</sup> Materials which expel the magnetic field are termed diamagnetic, whereas paramagnetic materials strengthen the field. Historically, molecules with a diamagnetic response to a magnetic field were called diatropic molecules, while molecules with paramagnetic response were termed paratropic.<sup>15</sup> However, nowadays these labels are only used for current-density pathways, since there are usually many diatropic and paratropic vortices in the same molecule.

## 5.5 Nuclear magnetic shielding

Atomic nuclei with non-zero spin give rise to a magnetic vector potential  $\mathbf{A}_{\text{nuc}}$ ,

$$\mathbf{A}_{\text{nuc}} = \frac{\mu_0}{4\pi} \frac{\mathbf{m}_{\text{nuc}} \times \mathbf{r}}{r^3}. \quad (5.14)$$

In the presence of an external magnetic field, the total magnetic vector potential experienced by electron  $i$  becomes

$$\mathbf{A}_i = \frac{1}{2} \mathbf{B} \times \mathbf{r}_{i\mathbf{O}} + \frac{\mu_0}{4\pi} \sum_K \frac{\mathbf{m}_K \times \mathbf{r}_{iK}}{r_{iK}^3}, \quad (5.15)$$

where  $\mathbf{r}_{i\mathbf{O}}$  is the distance between point  $\mathbf{r}_i$  and the gauge origin, the index  $K$  spans

all nuclei,  $\mathbf{m}_K$  is the magnetic moment of nucleus  $K$ , and  $\mathbf{r}_{iK}$  is the distance between electron  $i$  and nucleus  $K$ . Adding the total magnetic vector potential in Eq. 5.15 to the molecular Hamiltonian leads to an expression for the coupling between the nuclear magnetic moment and the magnetically induced current density,<sup>6,11,12,16,17</sup>

$$E^{\mathbf{m}_K B} = - \int \mathbf{A}_{\text{nuc}}^K(\mathbf{r}) \cdot \mathbf{J}^B(\mathbf{r}) d\mathbf{r}. \quad (5.16)$$

The magnetically induced current density gives rise to a secondary magnetic field according to Biot-Savart's law,

$$\mathbf{B}_{\text{loc}} = \frac{\mu_0}{4\pi} \int \frac{\mathbf{r} \times \mathbf{J}^B(\mathbf{r})}{r^3} d\mathbf{r}. \quad (5.17)$$

Hence, at every point in space, the magnetic field is the sum  $\mathbf{B} = \mathbf{B}_{\text{ext}} + \mathbf{B}_{\text{loc}}$ , which can also be expressed as

$$\mathbf{B}_{\text{loc}} = (1 - \sigma) \mathbf{B}, \quad (5.18)$$

where  $\sigma$  is the trace of the nuclear magnetic shielding tensor. Nuclear magnetic shieldings can be probed in nuclear magnetic resonance (NMR) spectroscopy, where the magnetic shielding constants of the nuclei are compared to a reference. The nuclear magnetic shieldings  $\sigma$  and the NMR chemical shifts  $\delta$  relative to the reference are small and reported in parts per million (ppm).

## 5.6 Nuclear magnetic shieldings and current densities

Nuclear magnetic shieldings can be calculated as the second derivative of the electronic energy with respect to the nuclear magnetic moment  $\mathbf{m}_K$  and the strength of the external magnetic field  $\mathbf{B}$ ,<sup>18</sup>

$$\sigma_{\alpha\beta}^K = \left. \frac{\partial^2 E^{\mathbf{m}_K B}}{\partial m_{\alpha}^K \partial B_{\beta}} \right|_{m_{\alpha}^K, B_{\beta}=0}, \text{ where } \alpha, \beta \in \{x, y, z\}. \quad (5.19)$$

Jameson and Buckingham showed that NMR shieldings can alternatively be obtained by differentiating the Biot-Savart expression in Eq. 5.16 with respect to the magnetic field and the nuclear magnetic moment.<sup>6,11,12,16,17,19</sup>

$$\sigma_{\alpha\beta}^K = -\frac{\mu_0}{4\pi} \sum_{\gamma\delta} \varepsilon_{\alpha\delta\gamma} \int \frac{r_{\delta} - R_{K\delta}}{|\mathbf{r} - \mathbf{R}_K|^3} \mathcal{J}_{\gamma}^{B_{\beta}}(\mathbf{r}) d\mathbf{r}, \quad (5.20)$$

where  $\alpha, \beta, \gamma, \delta$  are Cartesian directions,  $\epsilon_{\alpha\delta\gamma}$  is the Levi-Civita symbol,  $\mathbf{R}_K$  the distance from nucleus  $K$ . The advantage of the latter approach is that NMR shieldings can be analysed by studying the spatial contributions to them. Orbital contributions to the NMR shieldings can also be unambiguously calculated by determining orbital contributions to the current density and integrating their contributions to the Biot-Savart expression of the NMR shieldings.<sup>20,21</sup> The integrand, which is called the magnetic shielding density,<sup>17</sup> can be visualised, yielding a rigorous physical basis for interpreting NMR shieldings. The magnetic shielding density of a carbon atom in benzene is shown in Fig. 1(a) where one sees that the  $1s$  core electrons of the carbon shield the magnetic field at the nucleus. The nucleus is surrounded by a more distant deshielding region which in turn is embedded in a diffuse shielding region due to contribution from the electrons near the other atoms as well as from the electrons of the  $\sigma$  bonds and the conjugated  $\pi$  sextet. The shielding density of the hydrogen atom in benzene is illustrated in Fig. 1(b). The inner part of the  $1s$  orbital of the hydrogen is deshielding the nucleus, whereas shielding regions are found outside the hydrogen and along the C–H bond. The alternating shielding and deshielding contributions from the other carbon atoms are due to their atomic current densities.

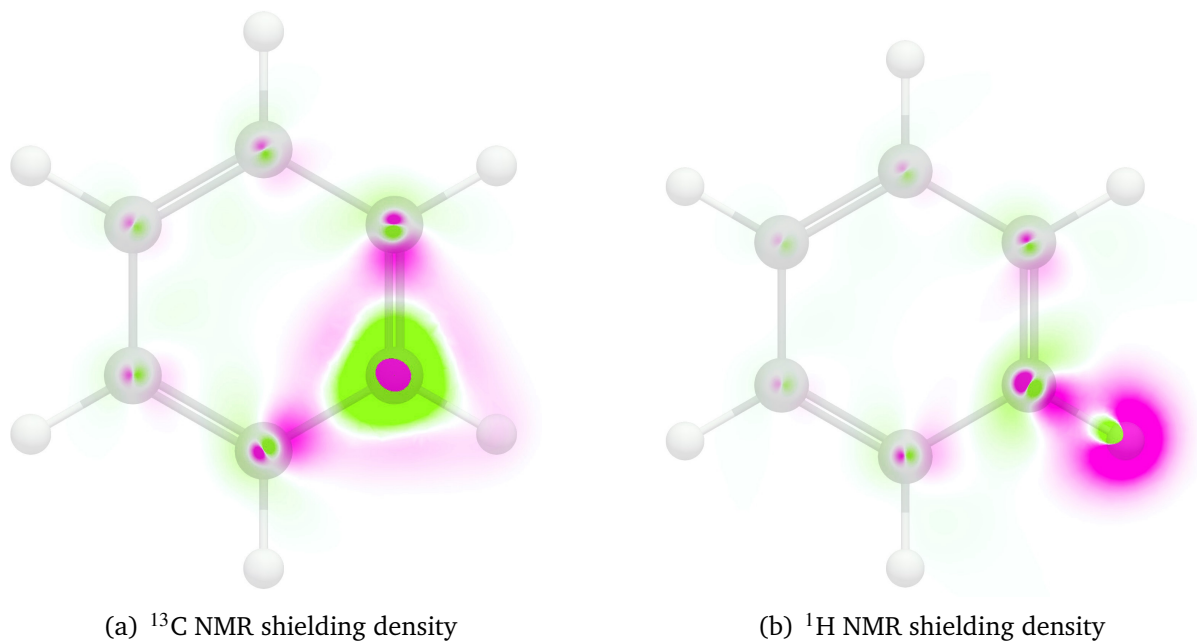


**Figure 1** The spatial contributions to the  $^{13}\text{C}$  NMR shielding density (left) and the  $^1\text{H}$  NMR shielding density (right) in the molecular plane of benzene. Shielding and deshielding contributions are shown in pink and green, respectively.

The contributions to the shielding density from each orbital can be obtained by partitioning the magnetic shielding tensor into localised orbitals. However, it leads to

mixing of occupied orbitals,<sup>22</sup> which results in unphysical orbital contributions when the orbital mixing is not prevented by symmetry. For planar molecules one can divide magnetic shieldings into  $\sigma$  and  $\pi$  contributions, since unitary transformations do not mix  $\sigma$  and  $\pi$  orbitals.<sup>21,23</sup>

## 5.7 Magnetic susceptibilities and closed-shell paramagnetic molecules

The magnetic susceptibility  $\chi_{\alpha\beta}$  with  $\alpha, \beta = \{x, y, z\}$ , also known as magnetisability, is the second derivative of the electronic energy with respect to the external magnetic field,<sup>24</sup>

$$\chi_{\alpha\beta} = - \left. \frac{\partial^2 E^{\mathbf{B}\mathbf{B}}}{\partial B_\alpha \partial B_\beta} \right|_{B_\alpha=0, B_\beta=0} \quad \text{with} \quad E^{\mathbf{B}\mathbf{B}} = - \int \mathbf{A}^{\mathbf{B}}(\mathbf{r}) \cdot \mathbf{J}^{\mathbf{B}}(\mathbf{r}) d\mathbf{r}, \quad (5.21)$$

where  $\mathbf{A}^{\mathbf{B}}(\mathbf{r})$  is the vector potential of the external magnetic field. Magnetisability is a second-rank tensor that similarly to the nuclear magnetic shielding,  $\sigma$ , can formally be divided into diamagnetic and paramagnetic contributions,<sup>25</sup>

$$\chi_{\alpha\beta} = \chi_{\alpha\beta}^{\text{d}} + \chi_{\alpha\beta}^{\text{p}} = \begin{cases} -\frac{1}{4} \sum_i \langle \Psi_0^{(0)} | \mathbf{r}_{\mathbf{O}i}^2 \delta_{\alpha\beta} - \mathbf{r}_{\mathbf{O}i,\alpha} \mathbf{r}_{\mathbf{O}i,\beta} | \Psi_0^{(0)} \rangle \\ + \frac{1}{2} \sum_{j \neq 0} \frac{\langle \Psi_0^{(0)} | (\hat{\mathbf{r}}_{\mathbf{O}i} \times \hat{\mathbf{p}}_i)_\alpha | \Psi_j^{(0)} \rangle \langle \Psi_j^{(0)} | (\hat{\mathbf{r}}_{\mathbf{O}i} \times \hat{\mathbf{p}}_i)_\beta | \Psi_0^{(0)} \rangle}{E_j^{(0)} - E_0^{(0)}} \end{cases} \quad (5.22)$$

where  $\mathbf{r}_{\mathbf{O}i}$  is the distance vector from a common gauge origin,  $\hat{\mathbf{p}}_i$  is the momentum operator of electron  $i$ , and the energies  $E_0^{(0)}$  and  $E_j^{(0)}$  are the unperturbed energies of the ground state and the  $j^{\text{th}}$  excited state, respectively.

The diamagnetic term depends only on the ground-state wave function and it is always negative, whereas the paramagnetic contribution that is expressed as a sum-over-states expression in Eq. 5.22 may be positive or negative. Most molecules are diamagnetic with a negative magnetisability, because the diamagnetic term dominates. Open-shell molecules might be paramagnetic due to contributions from the spin of the electrons, whereas a few closed-shell molecules are paramagnetic due to a very large positive contribution from the paramagnetic term in Eq. 5.22.<sup>26,27</sup> Magnetisability can also be expressed using the current-density susceptibility,  $\mathcal{J}_\gamma^{B_\beta}(\mathbf{r})$ ,

$$\chi_{\alpha\beta} = \frac{1}{2} \sum_{\delta\gamma} \varepsilon_{\alpha\delta\gamma} \int r_{\delta} \mathcal{J}_{\gamma}^{B_{\beta}}(\mathbf{r}) d\mathbf{r}, \quad (5.23)$$

where  $\varepsilon_{\alpha\delta\gamma}$  is the Levi-Civita symbol.<sup>11</sup> Contributions from the diatropic current density are negative, whereas paratropic current-density vortices have positive contributions to the magnetisability. The size of the positive contribution depends on the strength of the paratropic ring current and its radius. Antiaromatic porphyrins can be closed-shell paramagnetic molecules provided that the strength of the paratropic ring current be strong enough.<sup>28</sup>

Experimental magnetisabilities are the trace of the magnetisability tensor. For ring-shaped molecules, the external magnetic field induces a ring current in the molecular ring when the magnetic field has a vector component perpendicular to the ring. Planar aromatic and antiaromatic molecules are diamagnetic for the two other Cartesian components of the magnetic field. Thus, the paratropic ring current of antiaromatic molecules must be very strong in order to yield a paramagnetic contribution that cancels the diamagnetic ones arising from the other two magnetic field directions. Calculations on isophlorin and other antiaromatic porphyrinoids showed that the studied molecules become closed-shell paramagnetic when the strength of the paratropic ring current exceeds  $-20 \text{ nA} \cdot \text{T}^{-1}$ .<sup>29</sup> Calculations on expanded porphyrins such as expanded isophlorins with eight furan moieties connected by methine bridges and the corresponding structure with NH instead of O yielded strong paratropic ring currents and a large positive magnetisability due to the large radius of the paratropic ring current.<sup>28</sup> A large positive magnetisability has been measured for a closed-shell tetracationic hexaporphyrin nanowheel, which sustains a strong paratropic ring current of  $-65 \text{ nA} \cdot \text{T}^{-1}$  with a radius of  $13 \text{ \AA}$ .<sup>28,30</sup> Construction of paramagnetic porphyrinoid molecules with more than one paratropic ring-current pathway requires that each of the vortices sustain a paratropic ring current with a strength exceeding  $-20 \text{ nA} \cdot \text{T}^{-1}$ ,<sup>28</sup> since the diamagnetic contribution to the magnetisability scales about linearly with the size of the molecule according to Pascal’s rule.<sup>31</sup>

## 5.8 Treatment of the gauge origin in quantum chemistry

An important conclusion drawn by Keith and Bader is that the gauge origin need not be the same for all positions in space.<sup>9</sup> Gauge independence can be achieved, for example, by using different gauge origins for each point in space, as in the continuous translation

of the origin of the current density (CTOCD) methods<sup>11,32–40</sup> or by employing gauge-including atomic orbitals (GIAOs), also known as London orbitals.<sup>18,41–44</sup> GIAOs are physically meaningful since they involve a complex pre-factor in analogy with the one obtained by gauge transformations of wave functions. An ordinary Gaussian-type basis function  $\chi_K(\mathbf{r})$  centred on nucleus  $K$  is re-defined as  $\omega_K(\mathbf{r})$  with an explicit dependence on the magnetic vector potential of the external magnetic field  $\mathbf{A}_K^{\mathbf{B}}(\mathbf{r}) = \frac{1}{2}\mathbf{B} \times (\mathbf{R}_K - \mathbf{O})$  with its gauge origin at the nucleus as

$$\omega_K(\mathbf{r}, \mathbf{A}_K^{\mathbf{B}}) = \exp(-i\mathbf{r} \cdot \mathbf{A}_K^{\mathbf{B}}(\mathbf{r}))\chi_K(\mathbf{r}). \quad (5.24)$$

The wave function of a quantum system exposed to an external magnetic field is not gauge invariant because gauge transformations introduce a complex pre-factor to the wave function. The electronic interaction integrals as well as the electron density and the current density are gauge-origin independent,<sup>44</sup> which implies that molecular properties calculated as an expectation value of the electron density or obtained by integrating Biot-Savart expressions involving the current density are also independent of the chosen gauge function. The magnetically induced current density is gauge-origin independent when using GIAOs. Even though the current density has no reference to the gauge origin, the use of finite basis sets breaks the complete gauge invariance and leads to a leakage of the current density, *i. e.*, the charge conservation of the current density is not entirely fulfilled.<sup>45</sup>

## 5.9 The gauge-including magnetically induced current method

The expression for the nuclear magnetic shielding constant in Eq. 5.20 can be combined with the expression obtained by using analytical derivative theory. Rearrangement of the terms leads to an alternative expression for the current-density susceptibility.<sup>46–49</sup> Using the density matrix in the atomic-orbital (basis-function) basis,  $D_{\mu\nu}$ , and the magnetically perturbed density matrices,  $\frac{\partial D_{\mu\nu}}{\partial B_\beta}$ , yields the expression for calculating the current-density susceptibility which lies at the core of the gauge-including magnetically induced current method (GIMIC),



$$\begin{aligned}
\mathcal{J}_\alpha^{B_\beta}(\mathbf{r}) = & \sum_{\mu\nu} D_{\mu\nu} \frac{\partial \omega_\mu^*(\mathbf{r})}{\partial B_\beta} \frac{\partial \tilde{h}(\mathbf{r})}{\partial m_\alpha^K} \omega_\nu(\mathbf{r}) + \sum_{\mu\nu} D_{\mu\nu} \omega_\mu^*(\mathbf{r}) \frac{\partial \tilde{h}(\mathbf{r})}{\partial m_\alpha^K} \frac{\partial \omega_\nu(\mathbf{r})}{\partial B_\beta} \\
& + \sum_{\mu\nu} \frac{\partial D_{\mu\nu}}{\partial B_\beta} \omega_\mu^*(\mathbf{r}) \frac{\partial \tilde{h}(\mathbf{r})}{\partial m_\alpha^K} \omega_\nu(\mathbf{r}) - \sum_\delta \varepsilon_{\alpha\beta\delta} \sum_{\mu\nu} D_{\mu\nu} \omega_\mu^*(\mathbf{r}) \frac{\partial^2 \tilde{h}(\mathbf{r})}{\partial m_\alpha^K \partial B_\delta} \omega_\nu(\mathbf{r}),
\end{aligned} \tag{5.25}$$

where  $\omega(\mathbf{r})$  are the GIAOs as defined in Eq. 5.24 and  $\varepsilon_{\alpha\beta\delta}$  is the Levi-Civita pseudotensor. The magnetic interaction is represented by the operators

$$\frac{\partial \tilde{h}(\mathbf{r})}{\partial \mathbf{m}^K} = (\mathbf{r} - \mathbf{R}_K) \times \hat{\mathbf{p}} \quad \text{and} \tag{5.26}$$

$$\frac{\partial^2 \tilde{h}(\mathbf{r})}{\partial \mathbf{m}^K \partial \mathbf{B}} = \frac{1}{2} \left[ (\mathbf{r} - \mathbf{O}) \cdot (\mathbf{r} - \mathbf{R}_K) \mathbf{1} - (\mathbf{r} - \mathbf{O})(\mathbf{r} - \mathbf{R}_K) \right] \tag{5.27}$$

where  $\mathbf{O}$  is the gauge origin and  $\mathbf{R}_K$  are the nuclear coordinates. The singular expression  $|\mathbf{r} - \mathbf{R}_K|^{-3}$  appearing in all terms cancels and has been omitted in Eqs 5.26 and 5.27. Even though the expression in Eq. 5.25 seems to depend on both the gauge origin and the coordinates of the nuclear positions, they cancel and the dependences vanish.

For open-shell systems, it is possible to write two separate equations like Eq. 5.25 for calculating the orbital contributions to the current-density susceptibility from the spin-up ( $\alpha$ ) or spin-down ( $\beta$ ) electrons.<sup>50</sup> The expression in Eq. 5.25 is independent of the employed computational level because the many-body information from the electronic-structure calculation is compressed into the density matrix and the magnetically perturbed density matrices. Keith has derived an alternative expression for calculating current densities at the Hartree-Fock level using GIAOs.<sup>51</sup>

The GIMIC method has been implemented and is available for download from GitHub.<sup>52</sup> It is interfaced to commonly used quantum-chemistry program packages including Turbomole,<sup>53</sup> Gaussian,<sup>54</sup> Dalton<sup>55</sup> and Cfour<sup>56</sup>. GIAOs improve the basis-set convergence, which avoids the need to use very large basis sets. Leakage of the current density and charge conservation problems are very small even when using rather small basis sets of double- $\zeta$  polarisation quality, rendering current-density studies on very large molecules consisting of more than 2000 atoms feasible.<sup>57</sup>

## 5.10 Investigating current-density pathways in molecules

Magnetic fields induce current densities in all atoms and molecules. For example, when the magnetic field is pointing along the C–C bond in ethane, atomic and bond vortices can be identified, as well as the global diatropic current-density flux along the perimeter of the molecule, as shown in Fig. 2. Such global diatropic current-density pathways exist in all molecules.<sup>8</sup>

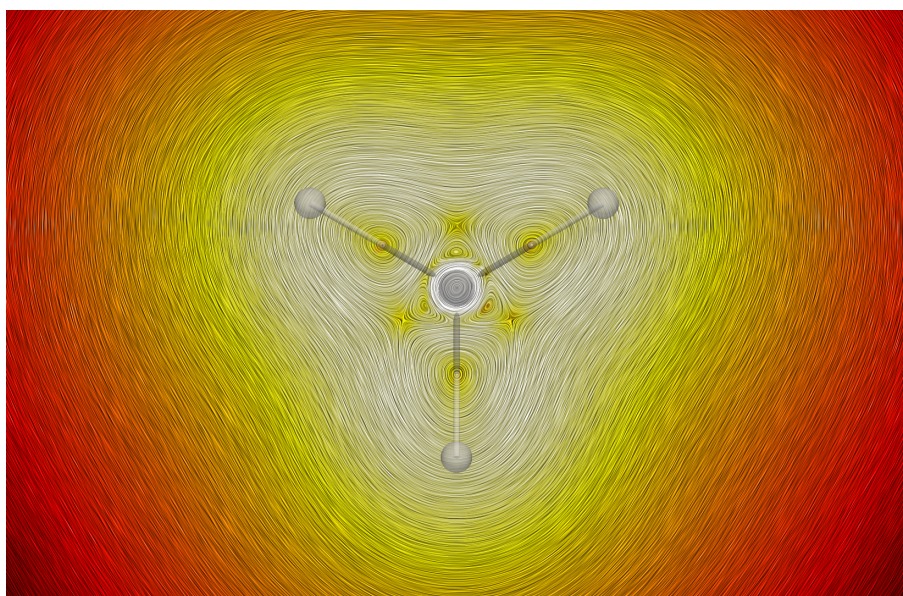


**Figure 2** The current-density susceptibility of ethane in a plane perpendicular to the C–C bond that crosses the nucleus of a carbon atom. The colour scale is logarithmic and it gives the strength of the modulus of the current-density susceptibility in the range of  $[3.57 \times 10^{-6}; 0.71] \text{ nA} \cdot \text{T}^{-1} \cdot \text{\AA}^{-2}$ .

Cyclic molecules are of interest in studies of magnetic properties, since aromatic and antiaromatic species can be potentially useful in solar cells, opto-electronics and as building blocks in conductive materials. The degree of aromaticity can be estimated from the strength of the ring-current (susceptibility) according to the ring-current model.<sup>41,58–61</sup> The aromatic ring-current model is nowadays an accepted concept even though illustrations of ring currents shown in textbooks are often oversimplified.<sup>62</sup>

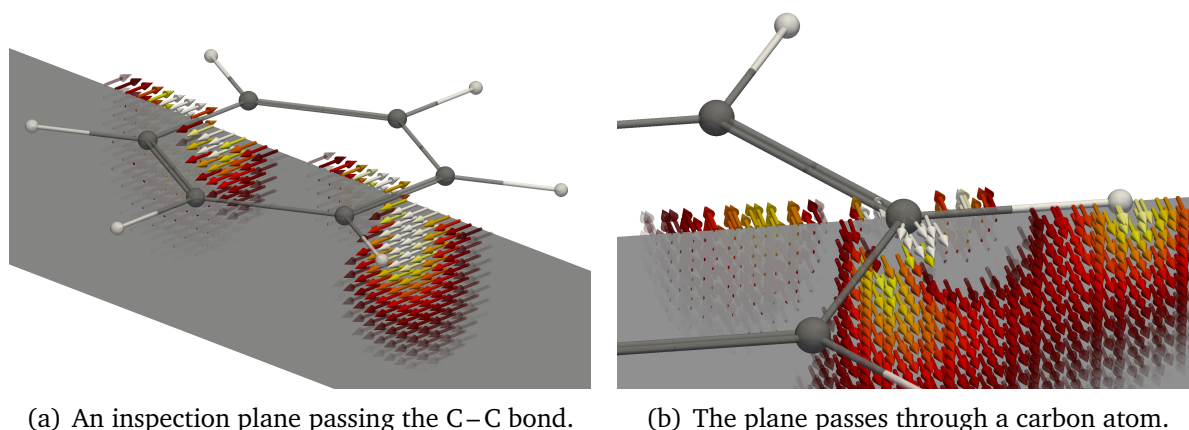


**Figure 3** Cross-sections of the magnetically induced current-density field in benzene. The molecule lies in the  $(x,y)$  plane and the magnetic field points in the  $z$  direction. Arrows show the direction of the magnetically induced current density. The colour scale indicates the strength of the current density.

The current-density susceptibility of benzene in a cross-section perpendicular to the molecular plane is illustrated in Fig. 3. Arrows show the direction of the current-density flux. The colour scheme reflects the strength of the current-density susceptibility. Note that we will use the term *current density* in the discussion below when referring to the *current-density susceptibility*. For weak magnetic fields, the current density is equal to the current-density susceptibility multiplied by the magnetic field strength. In the exterior of the molecule, there is a clockwise global diatropic current-density pathway, while inside the benzene ring, there is a paratropic ring current following the counter-clockwise direction. The cross-section of the ring current of benzene induced by a magnetic field perpendicular to the benzene ring is shown in the right part of the picture in Fig. 4 as well as in Fig. 3. The cross-section of the diatropic ring current is crescent-shaped on the outside of the carbon atoms and the paratropic ring current is seen inside the ring. The ring current is strong also in the molecular plane.

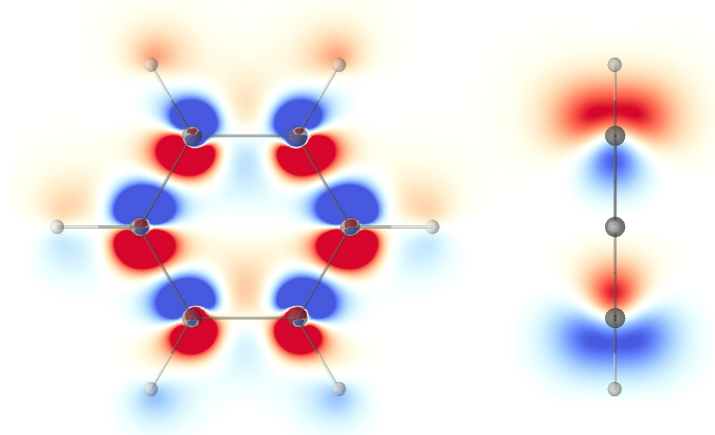
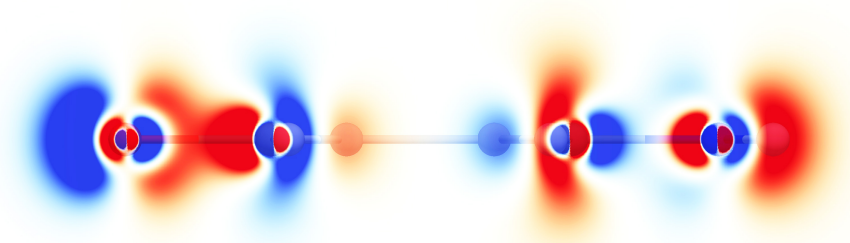


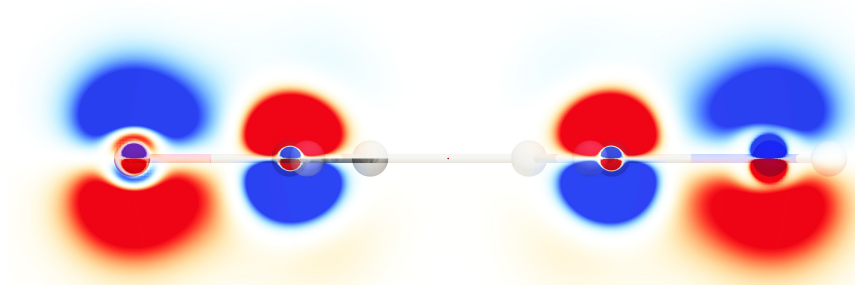
**Figure 4** The current density in the benzene molecule. The magnetic field is parallel to the molecular plane of the benzene molecule to the left and perpendicular to the molecular plane of the benzene molecule on the right. The strength the current density is in the range of  $[3.57 \times 10^{-6}; 0.43]$   $\text{nA} \cdot \text{T}^{-1} \cdot \text{\AA}^{-2}$  where blue areas show the current-density flux towards the reader, and the current-density flux away from the reader is shown in red.

The ring current gives rise to the diffuse shielding and deshielding regions shown in Fig. 1. The tropicity does not determine whether the current density shields or deshields the nucleus. Rather, this depends on the relative direction of the current density with respect to the nucleus under consideration. Similarly, the atomic current-density vortices of the other carbon atoms cause both shielding and deshielding based on the relative direction of the current density. The relative circulation direction of the global paratropic ring current inside the ring with respect to the carbon nucleus is the same as the one for the diatropic ring current, leading to a shielding contribution even though the inner contribution to the ring current is paratropic.

The pathways of the current-density flux depend on the direction of the magnetic field due to the presence of the angular momentum operator in the expression for the current density in Eq. 5.11. Thus, due to the molecular symmetry, there is no paratropic ring current in the benzene ring when the magnetic field is parallel to the molecular ring as illustrated for benzene in Fig. 4. Atomic current-density vortices with different spatial distribution and strength exist regardless of the direction of the magnetic field. The same also holds for  $\sigma$  bonds due to their local cylindrical symmetry along the bond axis.



(a) The magnetic field is perpendicular to the ring ( $B_{\perp}$ )



(b) The magnetic field is parallel to the ring ( $B_{\parallel}$ )

**Figure 5** The current density of *p*-aminophenol in an external magnetic field (a) perpendicular to the benzene ring; (b) parallel to the benzene ring. The OH group is on the left-hand side of the picture and the NH<sub>2</sub> group is to the right. The current-density flux pointing towards the viewer is illustrated in red, while the blue areas show the current density flowing away from the viewer.

Current-density vortices have the shape of a distorted torus, whose axis points more or less in the same direction as the magnetic field. In Fig. 5, a plane is positioned such that it crosses the oxygen and the nitrogen atoms of *p*-aminophenol with the magnetic field either perpendicular to the benzene ring or parallel to the line connecting the heteroatoms. The diatropic ring current at the carbon atoms with the substituents and the paratropic ring current inside the benzene ring are shown in Fig. 5(a). The current-density flux is also seen in the molecular plane. The OH and NH<sub>2</sub> substituents sustain a strong current density. There are several atomic vortices with different tropicity embedded in each other like onion shells. The atomic vortices are spatially larger when the magnetic field is parallel to the molecular plane, since in the perpendicular direction, there are also strong global current-density pathways on the outside of the molecule and inside the molecular ring. The direction of the current density in the valence orbitals of the atoms alternates when the magnetic field is parallel to the benzene ring.



Streamline plots are a useful visualisation tool as an analogue to classical trajectories. The Runge-Kutta method as implemented in Paraview<sup>63</sup> can be used in studies of the current-density flux calculated on a 3D grid. Streamline plots are employed to illustrate the effect of heteroatoms in the 2H-1,2-azaborolium cation, 1,3-imidazole and 2,5-dihydro-1H-1,2,5-azadiborole in Fig. 6. There are strong vortices around each nitrogen atom and the N – C bonds, which resemble the local current-density pathways found in porphyrinoids.<sup>64</sup>

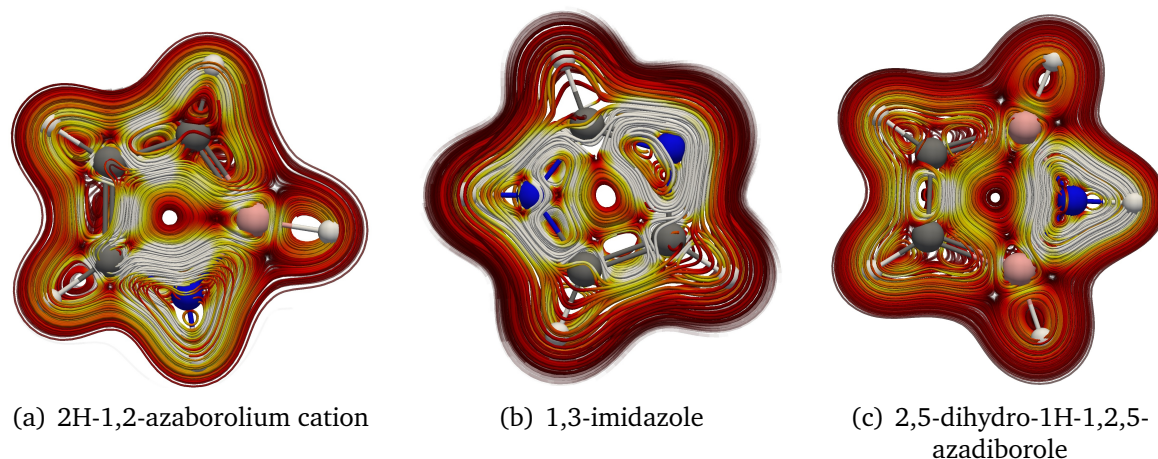


**Figure 6** The current densities of the 2H-1,2-azaborolium cation, imidazole and 2,5-dihydro-1H-1,2,5-azadiborole are illustrated with streamlines. The external magnetic field is perpendicular to the molecular plane. The colour scheme corresponds to the strength of the current density with white being the strongest.

### 5.11 Integrating the strength of the current density

Current density can be investigated by identifying the current-density pathways and determining their strengths by integrating the current-density flux through a plane as shown in Fig. 7(a). The origin of the integration plane is in the centre of the vortex and the plane extends far outside the molecular ring where the current density vanishes. In the vertical direction, the integration plane needs to be extended far enough where the current density vanishes. The same ring-current strengths are obtained regardless of whether the integration plane goes through a chemical bond or through an atom, because the current density formally fulfils the charge conservation condition. Small deviations can be obtained due to the use of finite basis sets. However, larger uncertainties are introduced for molecular rings with heteroatoms or for non-planar rings, since the axis of the current-density vortex is often shifted from the geometrical centre of the ring and bent with respect to the normal vector of the ring.

We employ a numerical integration scheme for calculating the strength of the current-density flux,  $I$ , which is obtained as<sup>46</sup>

$$I = \int_S \sum_{\beta} \frac{B_{\beta}}{|\mathbf{B}|} \hat{\mathcal{J}}^{B_{\beta}}(\mathbf{r}) \cdot \hat{\mathbf{n}} d\mathbf{s} \quad (5.28)$$

where the tensor elements of the current-density susceptibility  $\hat{\mathcal{J}}^{B_{\beta}}(\mathbf{r})$  are contracted with the three components of the external magnetic field, which is normalised to one.

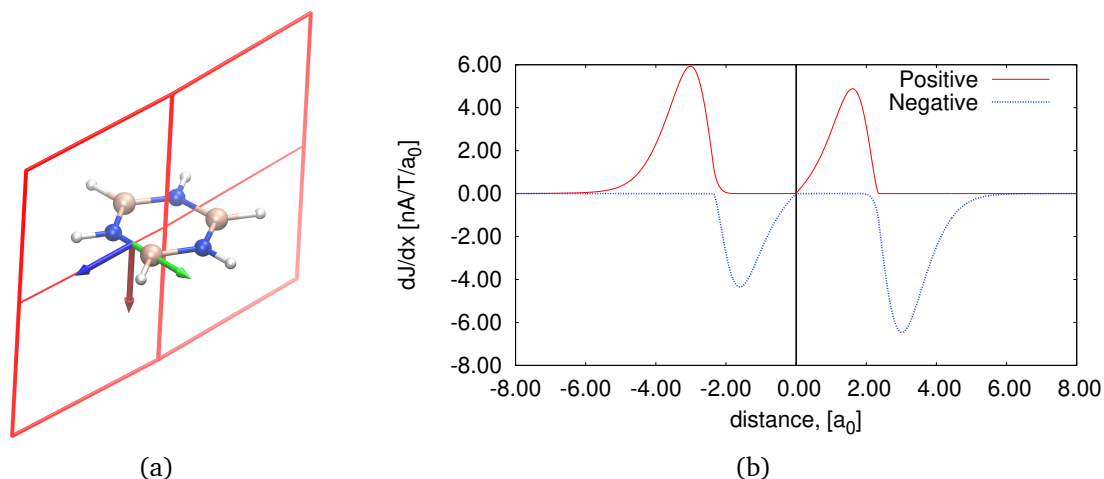


**Figure 7** (a) An integration plane is positioned in borazine such that it is perpendicular to the molecular plane and crosses a B–N bond. The basis vectors of the integration plane are shown as red, green and blue arrows. (b) The differential profile of the current density of borazine obtained by numerically integrating the current-density flux in thin vertical slices of the plane crossing the B–N bond and through the whole molecule. The net ring-current strength of borazine is  $3.23 \text{ nA} \cdot \text{T}^{-1}$ . The positive contributions refer to the current density, which seems to be flowing away from the viewer. The vertical bar at  $x = 0$  is the vortex origin. The values  $x < 0$  correspond to the left side of the integration plane shown in (a), while the right side of the plane with  $x > 0$  is the returning current on the other side of the vortex.

The strength of the current-density flux through the integration plane is then obtained as the scalar product of the current-density susceptibility for a given direction of the magnetic field,  $\hat{\mathcal{J}}^{B_{\beta}}(\mathbf{r})$ , and the normal of the integration plane,  $\hat{\mathbf{n}}$ .  $S$ . The external magnetic field is typically applied parallel to one of the axes of the integration plane. The strongest ring currents are obtained when the magnetic field is perpendicular to the molecular ring, *i. e.*, along the red arrow in Fig. 7(a). The SI unit for current density is  $\text{A} \cdot \text{T}^{-1} \cdot \text{m}^{-2}$  and we usually report strengths of ring-current susceptibilities in  $\text{nA} \cdot \text{T}^{-1}$ . We employ atomic units of distance, *i. e.*, bohr,  $1 a_0 = 0.529\,177\,210\,903(80) \text{ \AA}$ .

The direction of the current-density flux at the integration plane is used for assigning the tropicity of the current-density pathway. However, this assignment has to be considered with care because this simple algorithm cannot distinguish between diatropic current densities and returning paratropic current densities, and likewise, between paratropic

current-density fluxes and returning diatropic current-density fluxes. Current densities with a given tropicity have different directions when projected on the plane on the opposite sides of the vortex origin.

The profile of the strength of the current density at an integration plane through the geometric centre of borazine is shown in Fig. 7(b). The point  $x = 0$  marks the centre of the ring. The current density is integrated far out on both ends of the molecule. For monocyclic molecules, the positive contribution in one half of the molecule can be assigned as the diatropic ring current while the paratropic ring current appears as negative. For polycyclic molecules, the assignment of diatropic and paratropic ring-current contributions is difficult, especially when diatropic and returning paratropic ring currents mix as in naphthalene annelated with two pentalene moieties,<sup>65</sup> where the strongly antiaromatic pentalene units force the diatropic ring current of naphthalene to turn back, following the paratropic ring current inside its rings.

Thus, it is very important to have a clear visual understanding of the current-density flux before assigning the tropicity. Tropicity is a global property that can only be determined from the circulation direction with respect to the magnetic field vector by following the trajectories of the current-density vector field. For molecules consisting of fused rings, the assignment of the tropicity is complicated, because from the perspective of a given molecular ring, a paratropic vortex in an adjacent ring seems to be diatropic. When the tropicity is correctly assigned, diatropic current densities can be assumed to be positive and the paratropic ones are negative. The strength of the current-density flux is then the sum of the diatropic and paratropic contributions. A more detailed picture of the current-density flux can be obtained by separately investigating its diatropic and paratropic contributions rather than studying only the net strength.

## 5.12 The aromatic ring-current criterion

Electron delocalisation in the conjugated chemical bonds of aromatic molecules leads to an energetic stabilisation of the molecule correlating with the strength of the magnetically induced ring current.<sup>66–68</sup> Ring currents can be experimentally detected indirectly by measuring the anisotropy of the magnetic susceptibility<sup>41,58,59,69</sup> and <sup>1</sup>H NMR chemical shifts, which are, therefore, an important indicator of aromaticity. The <sup>1</sup>H NMR signals of the protons located on the exterior part of an aromatic ring are deshielded, leading to a downfield shift. The ring-current definition of aromatic molecules is that they sustain a net diatropic ring current when exposed to an external magnetic field,



whereas antiaromatic molecules sustain a net paratropic ring current.<sup>70</sup> Hückel's original  $\pi$ -electron counting rule states that molecular rings with  $(4n + 2)$   $\pi$  electrons are aromatic and that antiaromatic molecules have  $4n$   $\pi$  electrons.<sup>71–74</sup>

The existence of a strong current-density flux does not make a molecule aromatic or antiaromatic. Non-aromatic molecules sustain a weak net ring-current strength that may consist of strong diatropic and paratropic contributions canceling each other. The concept of aromaticity has been extended to triplet-state aromaticity,<sup>75</sup> the aromaticity of excited states<sup>76,77</sup> and of Möbius-twisted molecules.<sup>78–80</sup>

There are also other criteria to determine molecular aromaticity that are not always concordant.<sup>81</sup> For example, the magnetic and structural criteria for aromaticity correlate for aromatic Möbius-twisted hydrocarbon rings, whereas for the corresponding antiaromatic planar structures, the two aromatic criteria have opposite correlation.<sup>79</sup> Antiaromaticity does not always imply an increasing bond-length alternation.<sup>79,82–84</sup> The electron delocalisation of antiaromatic molecules resulting in paratropic ring currents leads to a less pronounced bond-length alternation than in non-aromatic molecules. Although the energetic criterion states that aromatic molecules are characterised by lower reactivity and greater chemical stability, this does not necessary imply that the lowest-energy conformer of a molecule is the most aromatic one according to the ring-current criterion.<sup>85</sup>

**Table 1** Calculated diatropic and paratropic contributions to the net ring-current strength susceptibility (in  $\text{nA} \cdot \text{T}^{-1}$ ) of benzene, the lowest singlet state of the benzene dication, and cyclohexadiene representing aromatic, antiaromatic, and non-aromatic molecules. The calculations were performed at the B3LYP/def2-TZVP level.

Molecule	Diatropic	Paratropic	Net current strength
Benzene <sup>a</sup>	17.00	-4.95	12.05
Benzene <sup>b</sup>	17.96	-6.20	11.76
Benzene <sup>2+</sup> <sup>a</sup>	2.57	-68.88	-66.32
Benzene <sup>2+</sup> <sup>b</sup>	6.42	-73.75	-67.33
Cyclohexadiene <sup>a</sup>	9.76	-10.25	-0.49
Cyclohexadiene <sup>b</sup>	7.92	-8.66	-0.74

<sup>a</sup> Through the middle of the C–C bond.

<sup>b</sup> Through the CH moiety.

Benzene is the archetypal aromatic molecule with 6  $\pi$  electrons fulfilling Hückel's rule for aromaticity. Benzene sustains a diatropic ring current of  $17.00 \text{ nA} \cdot \text{T}^{-1}$  in the  $\pi$  orbitals on both sides of the molecular ring as well as outside it. It sustains a paratropic

ring current of  $-4.95 \text{ nA} \cdot \text{T}^{-1}$  inside the ring. However, note that these values, as well as the other diatropic and paratropic contributions listed in Table 1 for the plane crossing the C–C bond also contain positive and negative contributions from the bond vortex. The net ring-current strength of  $12.05 \text{ nA} \cdot \text{T}^{-1}$  can be used as reference value for the degree of aromaticity of molecules.

The profile of the current density passing a plane in the middle of the C–C bond and a plane through the carbon and hydrogen atoms are shown in Fig. 8. Contributions to the ring current can be obtained by integrating the diatropic and paratropic domains separately. The actual paratropic contribution to the ring current of benzene is  $-3.38 \text{ nA} \cdot \text{T}^{-1}$ , which excludes contributions from other vortices. Integration of the sharp peak of the paratropic contribution yields the strength of the atomic current-density vortex of the carbon atom of  $2.0 \text{ nA} \cdot \text{T}^{-1}$ . The diatropic contribution calculated at the centre of the bond consists of the diatropic contribution to the ring current and the contribution from the diatropic bond vortex of  $1.6 \text{ nA} \cdot \text{T}^{-1}$ . The diatropic ring-current contribution is then  $16.4 \text{ nA} \cdot \text{T}^{-1}$ . Accurate contributions to the ring-current strengths can be obtained by integrating the often well-defined paratropic domains inside and near atoms, whereas in the middle of the bond, the paratropic contribution to the ring current and the contribution from returning diatropic current density of the bond vortex overlap.

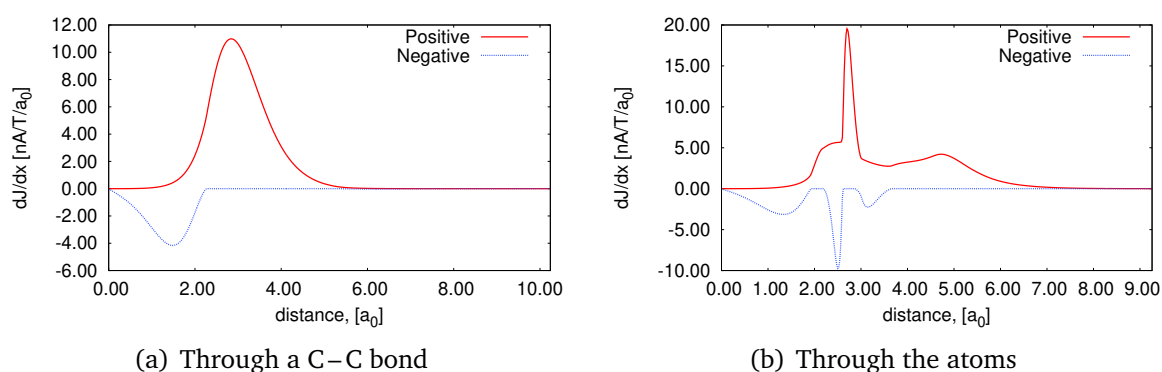


**Figure 8** The profile of the current-density susceptibility in benzene obtained by placing the integration plane (a) through a C–C bond; (b) through the C and H atoms.

The lowest singlet state of the benzene dication with  $4 \pi$  electrons fulfils Hückel's rule for antiaromaticity. It sustains a strong paratropic ring current of  $-66.32 \text{ nA} \cdot \text{T}^{-1}$  which consists of a diatropic contribution of  $2.57 \text{ nA} \cdot \text{T}^{-1}$  and a paratropic contribution of  $-68.88 \text{ nA} \cdot \text{T}^{-1}$ . The profiles of the integrated current density in planes through the middle of the chemical bond and through the CH moiety are shown in Fig. 9. The

current density is strongly paratropic inside the ring and it has a weak diatropic ring current outside the ring, which is typical for antiaromatic rings.<sup>62</sup> The current-density flux is always diatropic far away from the molecule,<sup>8</sup> even for strongly antiaromatic molecules. The ground-state of the benzene dication is a triplet state, whose molecular structure belongs to the  $D_{6h}$  point group like benzene.

Berger and Viel used group theoretical arguments to show that Jahn-Teller distorted molecules belonging to the  $C_n$ ,  $C_{nv}$ ,  $C_{nh}$ ,  $D_n$ ,  $D_{nh}$  for  $n > 2$ , and  $D_{nd}$  and  $S_{2n}$  for  $n > 1$  point groups are antiaromatic and applied their conclusions on cyclobutadiene and cyclooctatetraene.<sup>86</sup> They proposed a general symmetry principle for antiaromaticity that reads: “First-order and primoid second-order Jahn-Teller-distorted molecules out of non-isometric point groups are prone to induced paramagnetism in magnetic fields parallel to the main axis of symmetry”.<sup>86</sup> The antiaromaticity of the benzene dication belonging to the  $D_{2h}$  point group also follows the proposed symmetry principle.

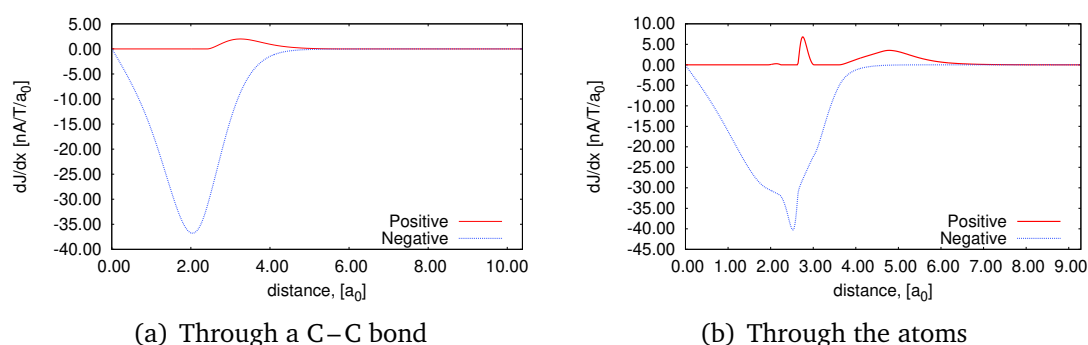


**Figure 9** The profile of the current-density susceptibility in the benzene dication obtained by placing the integration plane (a) through a C–C bond; (b) through the C and H atoms.

1,4-cyclohexadiene is a non-aromatic molecule. A diatropic current-density flux of  $9.76 \text{ nA} \cdot \text{T}^{-1}$  and a paratropic current-density flux of  $-10.25 \text{ nA} \cdot \text{T}^{-1}$  pass through a plane in the middle of the C=C double bond. The ring-current profiles in Fig. 10 show that the current density is diatropic outside the bond and paratropic inside it. The strengths of the diatropic and paratropic current densities are of the same size and cancel. In the integration profile through the CH moiety, one sees the paratropic current-density flux mainly inside the ring and the diatropic current-density flux passing on the outside of the carbon atom near the hydrogen. The sharp peaks are due to the atomic current-density vortex of the carbon atom. The diatropic and paratropic contributions to the current density are somewhat weaker when placing the integration plane through the CH moiety. This reveals that 1,4-cyclohexadiene has a strong current-density vortex at the C=C bond. The small difference in the net ring-current

strength of 1,4-cyclohexadiene is due to charge conservation problems. When using the larger quadruple- $\zeta$  basis sets augmented with polarisation and diffuse functions (def2-QZVPD),<sup>87,88</sup> the net ring-current strength of 1,4-cyclohexadiene is  $-0.57 \text{ nA} \cdot \text{T}^{-1}$  and  $-0.60 \text{ nA} \cdot \text{T}^{-1}$  through the bond and the CH moiety, respectively.

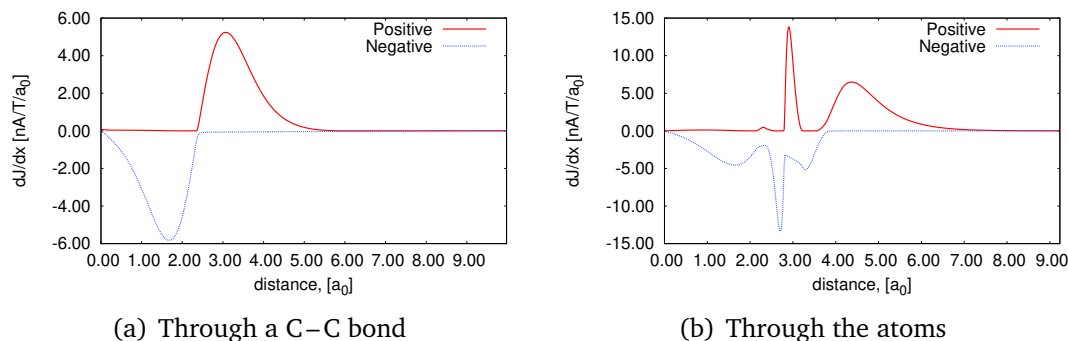


**Figure 10** The profile of the current-density susceptibility in 1,4-cyclohexadiene obtained by placing the integration plane (a) through a C–C bond; (b) through the CH moiety.

### 5.13 Aromatic pathways in polycyclic molecules

Determining the aromaticity of polycyclic aromatic hydrocarbons (PAH) and heterocyclic PAHs is complicated. The routes of the current-density flux can be determined by employing a variety of integration procedures that yield very detailed and reliable information about the current-density pathways in these molecules. Such calculations showed that a strong diatropic edge current dominates the current-density flux in ovalene,<sup>89</sup> whose molecular structure consists of a naphthalene moiety surrounded by eight benzene rings. The benzene rings at both ends of ovalene and those in the middle of the long sides of ovalene are Clar rings, sustaining a local ring current,<sup>90,91</sup> whereas the other benzene rings act as bridges that do not sustain any local ring current. Similar calculations on hexabenzocoronene showed that it sustains a global ring current around the edge of the molecule and the Clar rings sustain local ring currents.<sup>46,92,93</sup>

The current-density pathways in the heterocyclic PAHs shown in Fig. 11 are even more complicated. The seven-membered rings sustain local paratropic ring currents. The outer benzene rings sustain weak local diatropic ring currents and the rest of the rings act as bridges where the ring-current pathways split and join. A global diatropic ring current flows around the entire molecule, except at the paratropic seven-membered rings, where it takes the inner route, following the direction of the local paratropic ring current.

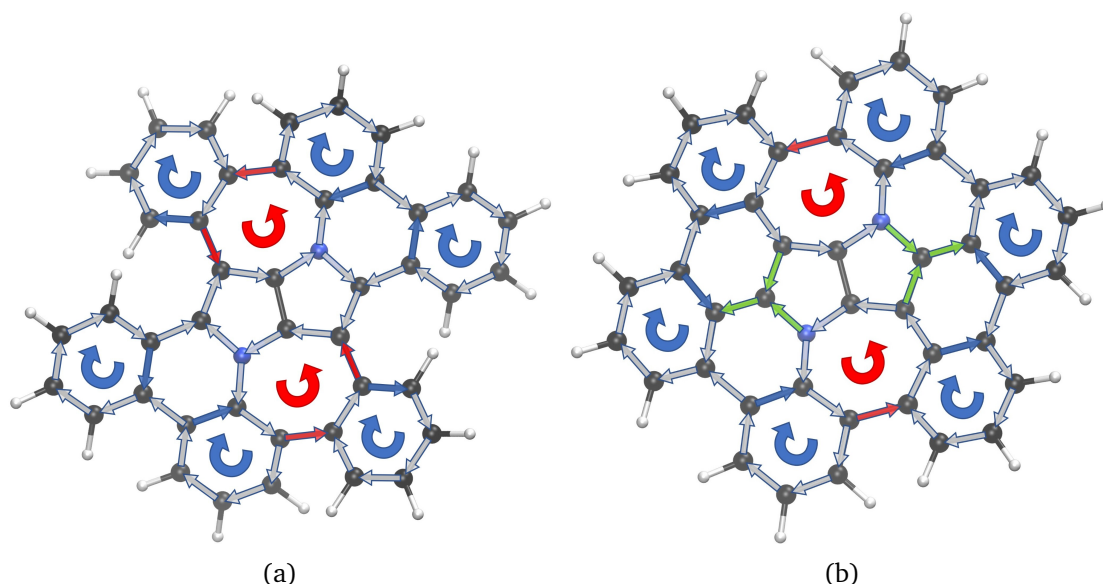


**Figure 11** The current-density pathways in (a) a heterocyclic hydrocarbon and (b) a fully conjugated nitrogen-embedded buckybowl.<sup>92,94</sup> The gray arrows show the global aromatic pathway. The red and blue arrows along the bonds indicate the local current-density fluxes. The green arrows show how the current-density flux splits and joins. The blue bent arrows denote local diatropic ring currents and the red ones show rings sustaining local paratropic ring currents.

Naphthalene with 10  $\pi$  electrons is aromatic, consisting of two annelated benzene rings. It sustains a ring current of  $12.60 \text{ nA} \cdot \text{T}^{-1}$  around the entire molecule. Inside each benzene ring, there is a local paratropic ring current which is distorted and tilted compared to the one of benzene. Naphthalene has a bond vortex in the  $\pi$  orbitals of the shared C–C bond as shown in Fig. 12(a). Its strength is about  $4.5 \text{ nA} \cdot \text{T}^{-1}$ . A better accuracy cannot be obtained without identifying the tropicity of the current-density vortices at the C–C bond.

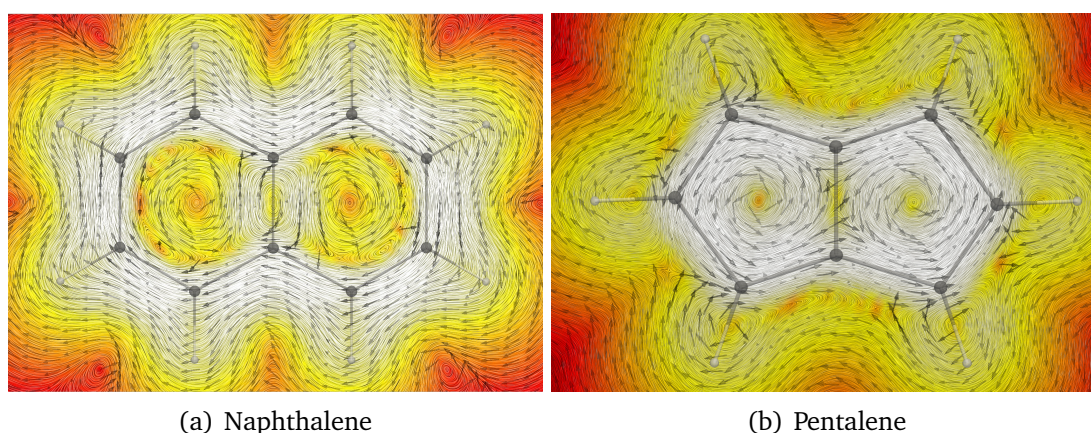


**Figure 12** The current density in naphthalene and pentalene in a plane positioned  $1 a_0$  above the molecular plane. The colour scale is logarithmic and gives the modulus of the strength of the current density in the range of  $[3.57 \times 10^{-6}; 0.54] \text{ nA} \cdot \text{T}^{-1} \cdot \text{\AA}^{-2}$ .

Pentalene, consisting of two annelated five-membered rings, is antiaromatic with 8  $\pi$  electrons. The current-density plot in Fig. 12(b) shows that the individual five-membered rings sustain strong paratropic ring currents mainly inside the ring. Pentalene exhibits also a global paratropic ring current around the entire molecule. The current-density flux is weakly diatropic along the outer edge of the molecule. The sum of the strengths of the local and the global paratropic ring currents is about  $-23 \text{ nA} \cdot \text{T}^{-1}$ , whereas the diatropic ring current is about  $3 \text{ nA} \cdot \text{T}^{-1}$ . A more accurate division into diatropic and paratropic contributions is difficult without identifying the tropicity of the current density by following the vector flux.

### 5.14 Aromatic and antiaromatic porphyrinoids

The ring current of free-base porphyrin ( $\text{H}_2\text{P}$ ) is divided into an inner and an outer branch at the pyrrole rings as shown in Fig. 13(a), which means that all  $\pi$  orbitals participate in its ring-current pathways.<sup>95,96</sup> Calculations of the orbital contributions to the current density showed that the current density from four  $\pi$  electrons dominates the ring current of  $\text{H}_2\text{P}$ . The remaining 22  $\pi$  electrons do not contribute significantly to the ring current.<sup>39</sup> Integration of the ring-current strengths along different routes shows that the current-density pathway *via* the inner hydrogen atoms is slightly weaker than along the outer route. The ring currents along the inner and outer branch at the pyrrole rings without an inner hydrogen are of about the same strength.<sup>95,96</sup>

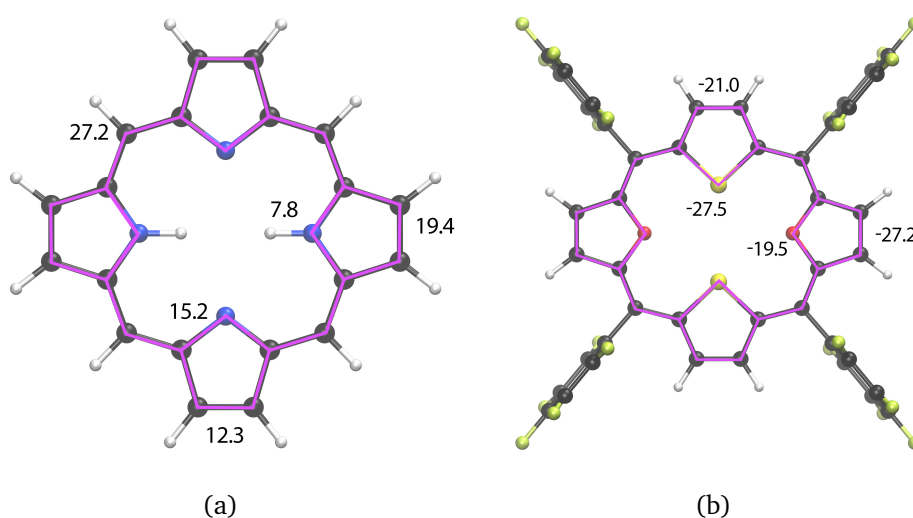


**Figure 13** The current-density pathways and ring-current strengths of (a) free-base porphyrin and (b) dioxo-dithiaaisophlorin with pentafluorophenyl substituents in the *meso* positions.

Individual current-density pathways can be identified by tracing the streamlines and



integrating the strength of the current density along different routes. GIMIC calculations account for the electronic response of the molecule to the external magnetic field and avoid assumptions of conjugation pathways, which is necessary when employing the semi-empirical annulene model.<sup>97</sup>

Isophlorin is a free-base porphyrin with four inner hydrogens fulfilling Hückel's rule for antiaromaticity. Isophlorin was predicted 60 years ago and air-stable isophlorins with four oxygen atoms or with two oxygen and two sulphur atoms replacing the inner NH moieties were recently synthesized.<sup>98–100</sup> Calculations of the current density of the synthesized isophlorins showed that they are indeed strongly antiaromatic, sustaining a strong paratropic ring current around the porphyrinoid ring.<sup>47,101</sup> The integrated ring-current strengths of dioxo-dithiaisophlorin in Fig. 13(b) show that the ring current is completely dominated by paratropic contributions. The ring current splits into inner and outer branches of almost equal strength at the furan and the thiophene rings. Thus, all  $\pi$  orbitals contribute to the ring-current pathway. The current-density flux of the outer pathways is slightly weaker than the inner ones. The current density is diatropic only at the outermost edge of the isophlorin ring, whereas paratropic current-density contributions completely dominate the inner part.<sup>96,101</sup>

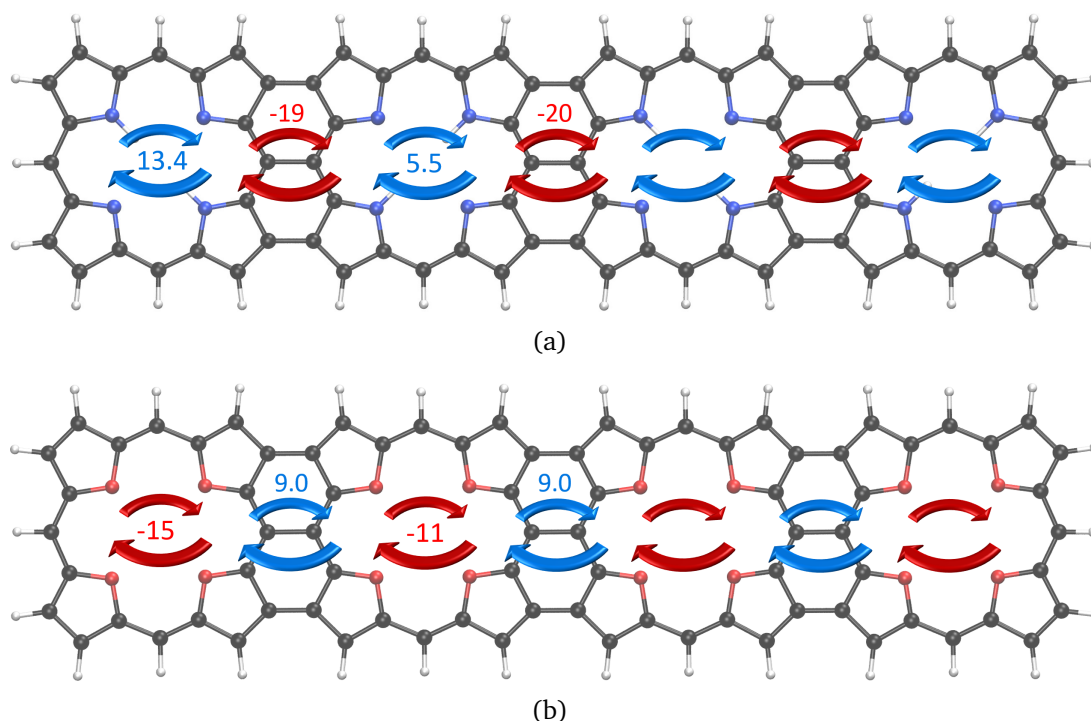


**Figure 14** Alternating diatropic and paratropic ring currents in annelated (a) porphyrin and (b) isophlorin arrays. The blue arrows denote the local diatropic ring currents and the local paratropic ones are marked with red arrows. The strengths of the local ring currents in  $\text{nA} \cdot \text{T}^{-1}$  are also given.<sup>28</sup>

Linear  $\beta$ - $\beta$ , *meso-meso*,  $\beta$ - $\beta$ -linked porphyrin arrays have been synthesized.<sup>102,103</sup> The

linking of the porphyrin rings leads to a molecular structure consisting of alternating porphyrin rings and naphthalene moieties as shown in Fig. 14(a). Current-density calculations showed that the porphyrin rings sustain diatropic ring currents, whereas the naphthalene-pyrrole moieties sustain paratropic ring currents.<sup>28</sup> The analogous linear  $\beta$ - $\beta$ , *meso-meso*,  $\beta$ - $\beta$ -linked isophlorin arrays shown in Fig. 14(b) have not been synthesized. Current-density analysis showed that the isophlorin arrays also have alternating ring currents with paratropic ring currents in the isophlorin rings and diatropic ring currents in the naphthalene rings.<sup>28</sup> Even though isophlorin is paramagnetic, the isophlorin arrays are diamagnetic, because the paratropic ring currents in the isophlorins are weaker than  $-20\text{ nA} \cdot \text{T}^{-1}$ , which is the lower threshold of the paratropic ring-current strength of closed-shell paramagnetic porphyrin rings.<sup>28</sup> The diatropic ring currents of the naphthalene moieties also increase the diamagnetic contribution to the magnetisability.<sup>28</sup> Large paramagnetic contributions would be needed from all isophlorin rings to make the isophlorin arrays paramagnetic, since the diamagnetic contribution to the magnetisability scales approximately linearly with the size of the molecule.<sup>31</sup>

## 5.15 Möbius-twisted molecules

The topology of twisted molecular rings is characterised by the linking number,  $L_k$ , which is equal to the sum of the twist  $T_w$  and the writhe  $W_r$ .<sup>104–107</sup>  $T_w$  is a local property, representing the one-dimensional twist of the molecular frame, whereas  $W_r$  is a measure of the global bending and deformation of the molecular ring in 3D space.<sup>80,108</sup>  $T_w$  and  $W_r$  can take any value for a given  $L_k$  as long the relation  $T_w + W_r = L_k$  is fulfilled.

A singly-twisted Möbius ring has an  $L_k$  value of  $1\pi$ , where  $\pi$  is often omitted for simplicity. Molecules with linking numbers of  $L_k$  and  $-L_k$  have the same topology but different chirality.<sup>80</sup> The Hückel rule for even-twisted Möbius molecules with  $|L_k| = 0, 2, 4, \dots$  states that a ring is aromatic when it has  $(4n + 2) \pi$  electrons in the ring, and antiaromatic with  $4n \pi$  electrons. The opposite rule holds for rings with an odd  $L_k$  value.



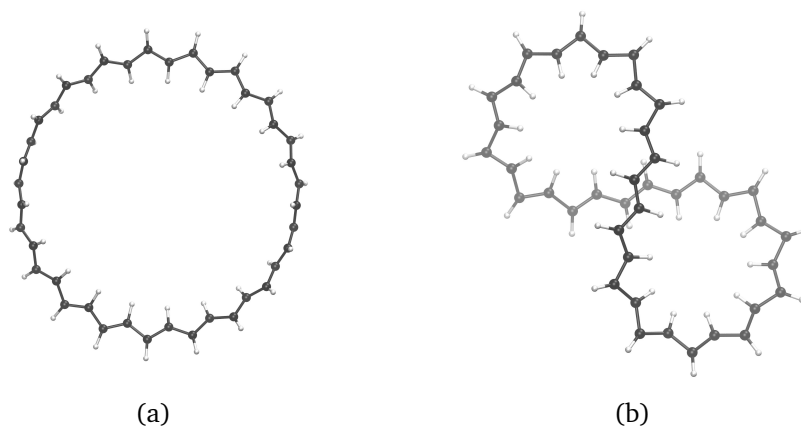


**Figure 15** (a) A planar double-twisted *trans*-C<sub>40</sub>H<sub>40</sub> ring with  $L_k = 2$ ,  $T_w = 2$  and  $W_r = 0$  and (b) a figure-eight-shaped *trans*-C<sub>40</sub>H<sub>40</sub> ring with  $L_k = 2$ ,  $T_w = 0.56$  and  $W_r = 1.44$ .

In Fig. 15, two doubly Möbius-twisted conformers of *trans*-C<sub>40</sub>H<sub>40</sub> are shown. The one with the shape of a circle is doubly twisted without writhe, whereas the figure-eight structure is less twisted but with a large writhe. Möbius-twisted molecules are generally non-planar which means that there is no obvious direction for the external magnetic field. The aromatic character can then be estimated by choosing the direction of the magnetic field that leads to the largest projection area of the ring, which is expected to yield the strongest ring-current strength.

Calculations on *trans*-annulene rings and their dications with a different topology showed that the strength of the ring current follows the generalised Hückel rule for Möbius-twisted molecules.<sup>108</sup> However, the degree of aromaticity depends strongly on the partitioning of  $L_k$  between  $T_w$  and  $W_r$ . The strongest ring currents were obtained for the most twisted molecules with the smallest  $W_r$ , regardless of whether the molecule is aromatic or antiaromatic. The most deformed rings with the largest  $W_r$  were found to be almost non-aromatic. The energetically lowest formally aromatic and antiaromatic molecules were the most twisted structures that also sustain the strongest diatropic and paratropic ring currents, respectively.

The first synthesized Möbius-twisted [16]annulene with  $L_k = 1$  was suggested to be aromatic based on spectroscopic studies.<sup>109</sup> However, calculations of the nucleus independent chemical shifts (NICS)<sup>110</sup> and ring-current strengths<sup>111</sup> showed that both the Möbius-twisted and the corresponding untwisted (Hückel) isomers are non-aromatic sustaining a ring current of about  $0.3 \text{ nA} \cdot \text{T}^{-1}$ . Due to the twist of the Möbius isomer, the carbon atoms at the opposite sides of the [16]annulene are close to each other, enabling the current density to make a weak through-space shortcut.<sup>111</sup>

Möbius-twisted expanded porphyrins with  $L_k = 1$  and  $L_k = 2$  have been synthesized.<sup>112,113</sup> Spectroscopic studies of molecules with a different number of  $\pi$  electrons suggested that the aromatic character of the synthesized hexaphyrins with  $L_k = 2$  follows the generalised Hückel rule for Möbius-twisted molecules.<sup>113,114</sup> Calculations of the current density of the doubly Möbius-twisted *meso*-trifluoromethyl-substituted hexaphyrins with formally 24, 26, 28 and 30  $\pi$  electrons showed that [26]hexaphyrin and [30]hexaphyrin are aromatic, sustaining diatropic ring currents, whereas [28]hexaphyrin is antiaromatic and [24]hexaphyrin is practically non-aromatic, sustaining a very weak paratropic ring current.<sup>115</sup> Singly Möbius-twisted monophosphorous complex of [28]hexaphyrin and bisphosphorous complex of [30]hexaphyrin were synthesized using phosphorous oxide (PO) moieties to force a single twist into the hexaphyrin ring.<sup>112</sup> The second PO introduces a strong twist ( $T_w = 1.72$ ), which is compensated by deforming the ring with a writhe of  $-0.72$ . The second PO unit also increases the number of  $\pi$  electrons in the conjugation pathway. The singly-twisted [28]hexaphyrin with  $L_k = 1$  is expected to be aromatic according to the generalised Hückel rule and [30]hexaphyrin is antiaromatic. The aromatic character of the singly-twisted hexaphyrins was confirmed by calculating the ring-current strength.<sup>116</sup> The paratropic ring current of the bisphosphorous complex of [30]hexaphyrin prefers the inner pathways but it also takes routes across the deformed molecular ring because the atoms on the opposite sides of the ring come close to each other due to the deformation of the ring.

## 5.16 Carbon nanostructures

### *Fullerene C<sub>60</sub>*

In the seminal work by Kroto *et al.*,<sup>117</sup> they stated that the inner and outer surfaces of C<sub>60</sub> are covered with a sea of  $\pi$  electrons and concluded that it appears to be aromatic. The aromatic character of fullerene (C<sub>60</sub>) has since then been debated. More recent studies of the aromaticity of fullerene have reached the conclusion that C<sub>60</sub> can hardly be considered aromatic.<sup>118–122</sup> Fullerene sustains local current-density vortices that lead to a strong diatropic current density on the outside and an equally strong paratropic current density on the inside resulting in a weak net ring current around the whole molecule.<sup>119,120</sup> Regardless of the direction of the magnetic field, C<sub>60</sub> has mainly local current-density vortices, which appear as white spots in Fig. 16.

The current density of C<sub>60</sub> is illustrated in Fig. 16 on a sphere with radius  $1 a_0$  larger

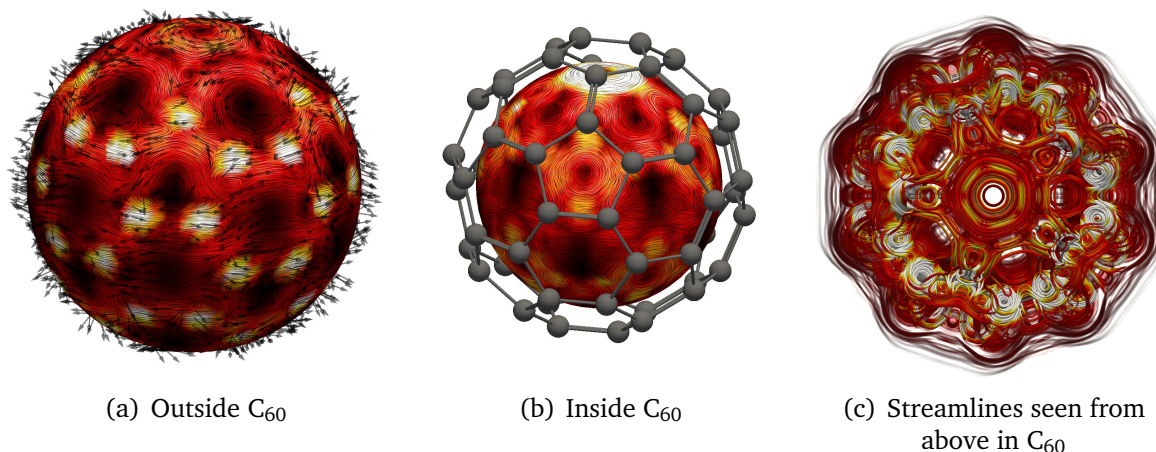


**Figure 16** The current density illustrated on a sphere with radius  $1 a_0$  larger (a) and small (b) than the surface of the  $C_{60}$  molecule, respectively. The colour scale indicates the strength of the current density in the range of  $[3.57 \times 10^{-6}; 0.54] \text{ nA} \cdot \text{T}^{-1} \cdot \text{\AA}^{-2}$ . (c) The current density in the middle of  $C_{60}$ .

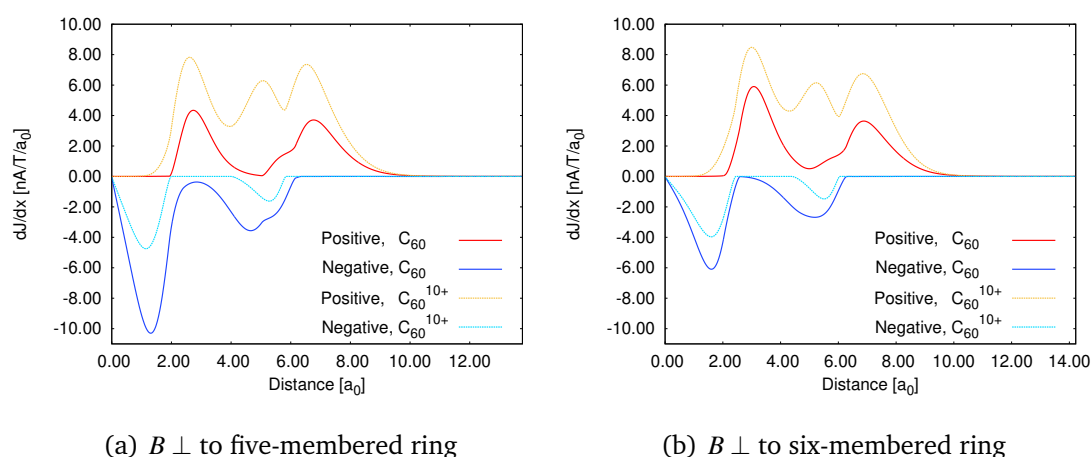


**Figure 17** The profile of the current density of  $C_{60}$  and  $C_{60}^{10+}$  when the magnetic field is perpendicular to (a) a five-membered ring (b) a six-membered ring.

and smaller than the radius of the molecular surface. The paratropic ring current inside  $C_{60}$  and the diatropic ring current outside it as well as the local vortices in the middle of the molecule are seen in Fig. 16(c).

The  $C_{60}$  fullerene fulfils the condition for spherical aromaticity when ten electrons are removed. Approximately spherical molecules are spherical aromatic when the number of  $\pi$  electrons is  $2(n+1)^2$ ,<sup>123–125</sup> which is analogous to the closed-shell configurations of pseudoatoms with a spherical shell potential.<sup>126</sup> Current-density calculations showed that  $C_{60}^{10+}$  is spherical aromatic sustaining strong diatropic contributions to the current density around the entire molecule.

The profile of the current density passing through the upper half of  $C_{60}$  and  $C_{60}^{10+}$  are shown in Fig. 17 where one sees that the current-density profiles are fairly independent

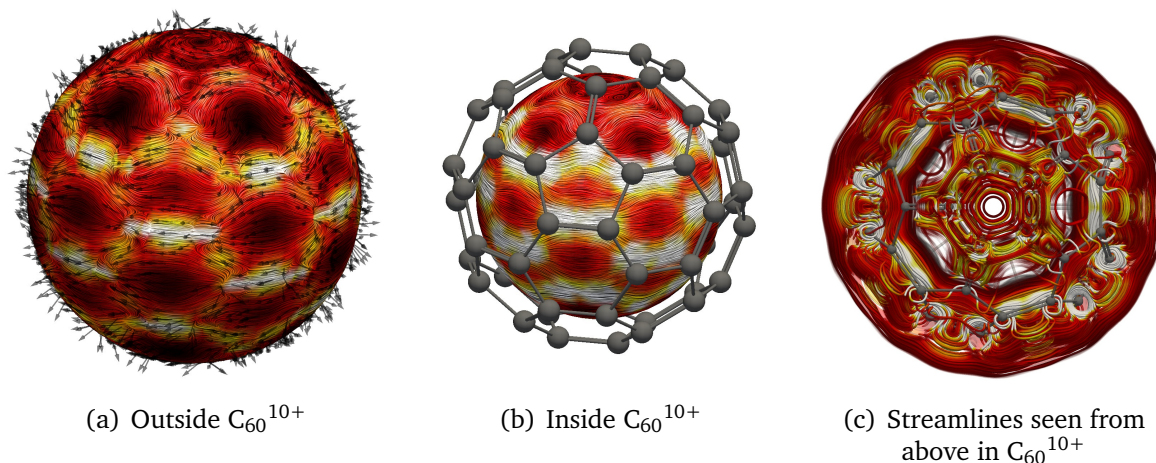


**Figure 18** The current density illustrated on a sphere with a radius  $1 a_0$  (a) larger and (b) smaller than the surface of the  $C_{60}^{10+}$  molecule. The colour scale indicates the strength of the current density in the range of  $[3.57 \times 10^{-6}; 0.54] \text{ nA} \cdot \text{T}^{-1} \cdot \text{\AA}^{-2}$ . (c) The current density in the middle of  $C_{60}^{10+}$ .

of the direction of the magnetic field. The local ring current in the five-membered rings of  $C_{60}$  is strongly paratropic when the magnetic field is perpendicular to that ring. There is a diatropic current-density flux in the six-membered ring adjacent to the five-membered one. When the magnetic field is perpendicular to a six-membered ring, it sustains a local paratropic ring current inside it as in benzene. The local paratropic ring current of the five-membered ring is much stronger than the one inside the six-membered one. Fullerene is non-aromatic, since it sustains alternating diatropic and paratropic contributions to the current density, whose strengths nearly cancel, whereas  $C_{60}^{10+}$  is dominated by a strong global diatropic current-density flux.

The current-density flux of  $C_{60}^{10+}$  is diatropic both inside and outside the carbon framework as seen in Fig. 18. The uniform diatropic current-density flux seen in Fig. 18(c) leads to a constant magnetic shielding inside the molecule like a magnetic Faraday cage.<sup>127</sup>

**Table 2** Calculated diatropic and paratropic contributions to the net ring-current strength susceptibility (in  $\text{nA} \cdot \text{T}^{-1}$ ) of  $\text{C}_{60}$ ,  $\text{C}_{60}^{10+}$  and gaudiene ( $\text{C}_{72}$ ). The calculations were performed at the B3LYP/def2-TZVP level.

Molecule	Diatropic	Paratropic	Net current strength
$\text{C}_{60}^a$	25.40	-41.50	-16.00
$\text{C}_{60}^b$	31.74	-26.46	5.26
$\text{C}_{60}^{10+, a}$	68.20	-14.26	43.84
$\text{C}_{60}^{10+, b}$	71.26	-13.22	58.04
$\text{C}_{72}^c$	56.82	-10.98	45.84

<sup>a</sup> The magnetic field is perpendicular to a five-membered ring.

<sup>b</sup> The magnetic field is perpendicular to a six-membered ring.

<sup>c</sup> The magnetic field is perpendicular to a four-sided equilateral twelve-membered ring.

### Gaudiene

The cavernous gaudiene ( $\text{C}_{72}$ ) molecule belonging to the  $O_h$  point group consists of two different kinds of conjugated twelve-membered rings.<sup>128–130</sup> One of them has alternating single, double and triple bonds and the other one is an equilateral four-sided ring with single, triple and single bonds along the sides. The molecular structure of gaudiene can formally be constructed from a truncated octahedron by replacing eight of the twelve edges of the octahedron with  $-\text{C}\equiv\text{C}-$  units.<sup>129</sup> Gaudiene is aromatic, sustaining a strong diatropic current-density flux of  $45.84 \text{ nA} \cdot \text{T}^{-1}$  around the cage structure. The net current-density flux was integrated by placing a plane through the whole molecule such that it begins at the centre of an equilateral twelve-membered and continues outwards.

Even though gaudiene with 72  $\pi$  electrons fulfils the  $2(n+1)^2$  rule of spherical aromaticity, it cannot be considered spherical aromatic because the current density mainly follows the carbon framework as shown in Fig. 19, rather than forming a uniform current density on both sides of the carbon framework as in the case of  $\text{C}_{60}^{10+}$ .<sup>129,130</sup> This is understandable, since the cavities of  $\text{C}_{72}$  are significantly larger than in fullerene that is constructed from five- and six-membered carbon rings.  $\text{C}_{72}$  also lacks dense horizontal pathways for the current density as in  $\text{C}_{60}^{10+}$ .

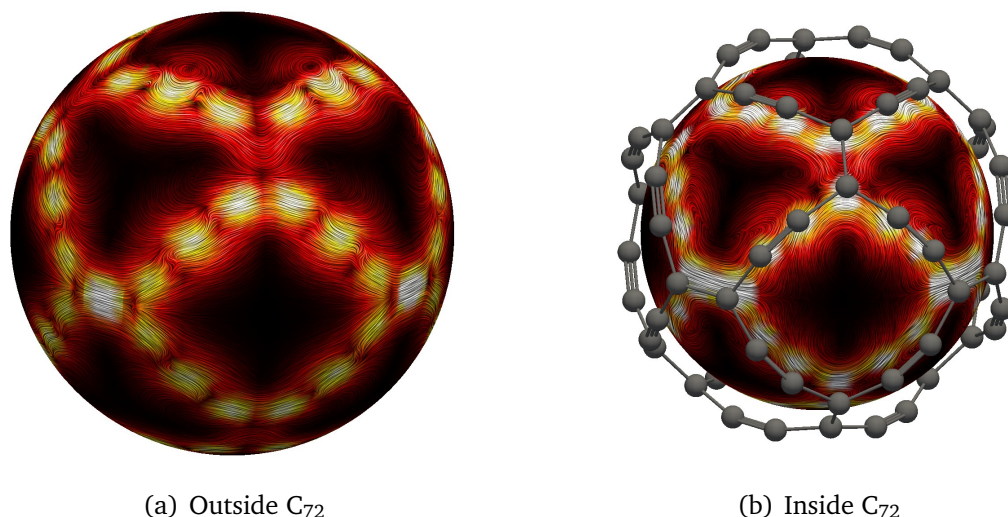


**Figure 19** The current density of gaudiene illustrated on the surface of a sphere at a distance of about  $1 a_0$  from the carbon framework (a) outside and (b) inside of the  $C_{72}$  the cage.

### *Toroidal carbon nanotubes*

Extensive computational and experimental studies of toroidal carbon nanotubes (TCNT) were initiated after they were observed and unequivocally confirmed.<sup>131–135</sup> The radii of the observed TCNTs are about 300 – 400 nm, which is too large for first-principle electronic structure calculations. TCNTs are expected to exhibit unusual magnetic properties due to their topology. An external magnetic field perpendicular to the major radius of the torus can induce a current-density flux around the perimeter of the torus. In chiral tori, the current-density pathways can also follow the nanotube forming the torus, giving rise to an induced toroidal magnetic field perpendicular to the applied one inside the nanotube. The induced magnetic field inside the volume of the torus along the axis of the nanotube has no north and south poles. The current density around the nanotube also leads to a magnetically induced anapole moment perpendicularly to the major radius of the torus.<sup>136–138</sup> Two enantiomers of chiral TCNTs have an opposite sign of the anapole moment.<sup>139</sup>

The magnetic properties of small TCNTs have been studied computationally.<sup>57,137,139–142</sup> Optimisation of the molecular structure of TCNTs show that the cross-section of the nanotube is elliptical, leading to reasonable C–C distances on the inside and the outside of the torus when the torus is large enough.<sup>57</sup> Reasonable C–C distances can be obtained for smaller TCNTs by introducing seven-membered rings inside the torus and five-membered rings on the outside of it.<sup>57,143</sup>

Current-density calculations on the chiral polyhex (6,3)  $C_{2016}$  TCNT showed that it sus-



tains a strong ring current of  $292 \text{ nA} \cdot \text{T}^{-1}$  along the nanotube forming the torus and an even stronger ring current of  $3307 \text{ nA} \cdot \text{T}^{-1}$  around it.<sup>57</sup> The current-density flux of  $\text{C}_{2016}$  is shown in Fig. 20. The chiral ring current around the nanotube results in an induced magnetic field along the axis of the nanotube and a magnetically induced anapole moment. Calculations of the magnetically induced current density of larger TCNTs are computationally expensive. The current density of large TCNTs can be studied by using the computationally cheaper pseudo- $\pi$  model, which is a model system where the carbon atoms are replaced with hydrogens.<sup>144</sup>

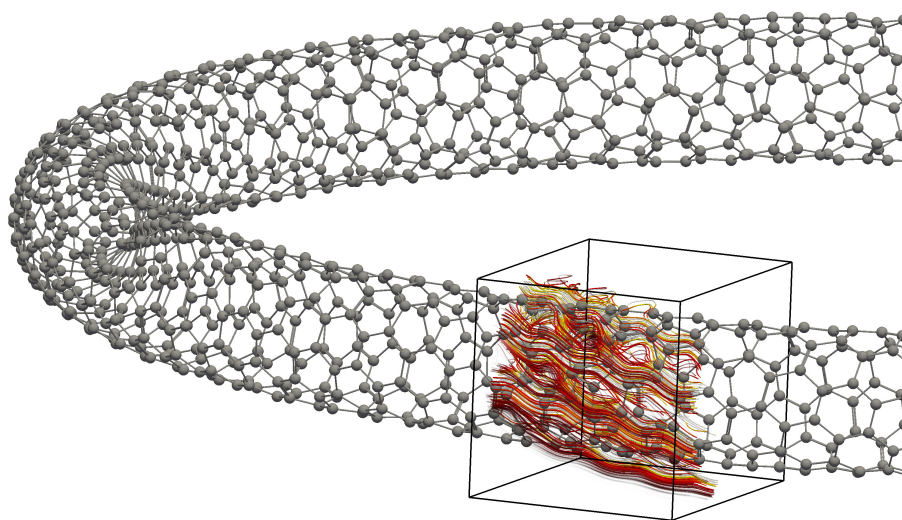


**Figure 20** The current density in the chiral polyhex (6,3) toroidal carbon nanotube  $\text{C}_{2016}$ .

## 5.17 Aluminium clusters

Metal clusters may also sustain ring currents when they are exposed to an external magnetic field. They can also be considered aromatic or antiaromatic in accordance with the ring-current criterion, which is acceptable as long as one is aware of the fact that aromaticity has a different meaning in organic chemistry.<sup>81,145</sup> For example, the synthesized  $\text{Al}_4^{2-}$  cluster is aromatic based on the tropicity and the strength of the magnetically induced current density.<sup>146–150</sup> The aluminium atoms in  $\text{Al}_4\text{Li}_2$  form a square-planar ring with a diatropic current-density vortex in the centre of the ring. The vortex reaches out to the outer edge of the  $\text{Al}_4$  ring where it becomes the global diatropic ring current. Integration of the current density from the centre of the ring through a bond and excluding the atomic current-density vortices of the lithium atoms yielded a net current strength of  $25.6 \text{ nA} \cdot \text{T}^{-1}$ , which is twice the net ring-current strength of benzene. No paratropic ring current was found. The  $\text{Al}_4^{4-}$  ring is rectangular with

alternating bond lengths, which suggests that it is antiaromatic. Current-density calculations at the coupled-cluster level of theory showed that the ring current has strong diatropic and paratropic contributions.<sup>148,150</sup> The paratropic contribution to the ring current is slightly stronger leading to a net paratropic ring-current strength of  $-3.1 \text{ nA} \cdot \text{T}^{-1}$  for  $\text{Al}_4\text{Li}_4$ , indicating that it is non-aromatic or weakly antiaromatic according to the ring-current criterion. The  $\text{Al}_4^{2-}$  ring is  $\pi$ - and  $\sigma$ -aromatic, whereas the  $\text{Al}_4^{4-}$  cluster sustains a diatropic ring current in the  $\sigma$  orbitals and a paratropic ring current in the  $\pi$  orbitals.<sup>148,150</sup>

## 5.18 Scope and limitations of the GIMIC method

The GIMIC method is a powerful method for interpreting different aspects of current-density susceptibilities and molecular magnetic properties. GIMIC is under active development with new features being planned and implemented continuously. The current-density susceptibility is a tensor function with nine components that are contracted to a vector function with three components when specifying a given direction of the external magnetic field. Vector functions are complicated to visualise and to analyse. We have developed and implemented novel computational and practical tools for interpreting calculated current-density susceptibilities. Orbital contributions to the current density are important, for example, when determining orbital contributions to nuclear magnetic shieldings. We plan to implement such features in future versions of the GIMIC code.

The current-density susceptibility consists of diatropic and paratropic contributions with opposite direction of rotation of the flux in the current-density vortex. The tropicity can be assigned by following the trajectories of the vector field, whereas in the present version of the GIMIC method, we use the direction of the current-density flux across an integration plane to assign the tropicity, which is an approximation that requires careful considerations.

Calculations with the GIMIC program can be performed at any level of theory, as long as the unperturbed and the magnetically perturbed density matrices are available. Current-density studies on large molecules are mainly performed at the DFT level. Calculations on aromatic organic molecules using traditional functionals like B3LYP<sup>151,152</sup> yield accurate strengths of the current-density flux, whereas functionals with a larger fraction of Hartree-Fock exchange should be used when studying magnetic properties of strongly antiaromatic molecules, because the B3LYP functional significantly overestimates the strength of their paratropic ring currents.<sup>101,153</sup> Similar conclusions have



been reached in recent comparisons of the degree of aromaticity calculated with different DFT functionals using a variety of aromaticity criteria.<sup>154–156</sup>

# Bibliography

- [1] Berger, R. J. F.; Monaco, G.; Zanasi, R. On the topology of total and diamagnetic induced electronic currents in molecules. *J. Chem. Phys.* **2020**, *152*, 194101.
- [2] Schrödinger, E. Quantisierung als Eigenwertproblem. *Ann. Phys.* **1926**, *386*, 109–139.
- [3] Hirschfelder, J. O. Quantum mechanical equations of change. I. *J. Chem. Phys.* **1978**, *68*, 5151–5162.
- [4] Heller, D. F.; Hirschfelder, J. O. Paramagnetic electronic properties and nodal topology. *J. Chem. Phys.* **1977**, *66*, 1929–1933.
- [5] Pelloni, S.; Lazzeretti, P. Ring current models for acetylene and ethylene molecules. *Chem. Phys.* **2009**, *356*, 153–163.
- [6] Lazzeretti, P.; Malagoli, M.; Zanasi, R. Computational approach to molecular magnetic properties by continuous transformation of the origin of the current density. *Chem. Phys. Lett.* **1994**, *220*, 299–304.
- [7] Fowler, P. W.; Steiner, E.; Havenith, R. W. A.; Jenneskens, L. W. Current density, chemical shifts and aromaticity. *Magn. Reson. Chem.* **2004**, *42*, S68–S78.
- [8] Gomes, J. A. N. F. Topological elements of the magnetically induced orbital current densities. *J. Chem. Phys.* **1983**, *78*, 4585–4591.
- [9] Keith, T. A.; Bader, R. F. W. Topological analysis of magnetically induced molecular current distributions. *J. Chem. Phys.* **1993**, *99*, 3669–3682.
- [10] Lazzeretti, P. Topological definition of ring currents. *Phys. Chem. Chem. Phys.* **2016**, *18*, 11765–11771.
- [11] Lazzeretti, P. Ring currents. *Prog. Nucl. Magn. Reson. Spectrosc.* **2000**, *36*, 1–88.
- [12] Lazzeretti, P. Current density tensors. *J. Chem. Phys.* **2018**, *148*, 134109.
- [13] Hirschfelder, J. O. The angular momentum, creation, and significance of quantized vortices. *J. Chem. Phys.* **1977**, *67*, 5477–5483.
- [14] Ricca, R. L. *Quantized Vortex Dynamics and Superfluid Turbulence*; Springer, 2001; pp 366–372.

- [15] Sondheimer, F. Annulenes. *Acc. Chem. Res.* **1972**, *5*, 81–91.
- [16] Jameson, C. J.; Buckingham, A. D. Nuclear magnetic shielding density. *J. Phys. Chem.* **1979**, *83*, 3366–3371.
- [17] Jameson, C. J.; Buckingham, A. D. Molecular electronic property density functions: The nuclear magnetic shielding density. *J. Chem. Phys.* **1980**, *73*, 5684–5692.
- [18] Wolinski, K.; Hinton, J. F.; Pulay, P. Efficient implementation of the gauge-independent atomic orbital method for NMR chemical shift calculations. *J. Am. Chem. Soc.* **1990**, *112*, 8251–8260.
- [19] McWeeny, R. Currents, kinetic energy, and molecular magnetism. *J. Chem. Sci.* **1986**, *96*, 263–273.
- [20] Steiner, E.; Fowler, P. W. On the orbital analysis of magnetic properties. *Phys. Chem. Chem. Phys.* **2004**, *6*, 261–272.
- [21] Acke, G.; Van Damme, S.; Havenith, R. W. A.; Bultinck, P. Interpreting the behavior of the NICS<sub>zz</sub> by resolving in orbitals, sign, and positions. *J. Comp. Chem.* **2018**, *39*, 511–519.
- [22] Bohmann, J. A.; Weinhold, F.; Farrar, T. C. Natural chemical shielding analysis of nuclear magnetic resonance shielding tensors from gauge-including atomic orbital calculations. *J. Chem. Phys.* **1997**, *107*, 1173–1184.
- [23] Orozco-Ic, M.; Celaya, C. A.; Sundholm, D. Calculation of magnetic response properties of tetrazines. *RSC Adv.* **2020**, *10*, 18124–18130.
- [24] Ruud, K.; Helgaker, T.; Bak, K. L.; Jørgensen, P.; Jensen, H. J. A. Hartree-Fock limit magnetizabilities from London orbitals. *J. Chem. Phys.* **1993**, *99*, 3847–3859.
- [25] Corcoran, C. T.; Hirschfelder, J. O. The magnetic susceptibility of BH. *J. Chem. Phys.* **1980**, *72*, 1524–1528.
- [26] Stevens, R. M.; Lipscomb, W. N. Perturbed Hartree-Fock Calculations. V. Magnetic Properties of the BH Molecule. *J. Chem. Phys.* **1965**, *42*, 3666–3669.
- [27] Pelloni, S.; Lazzeretti, P.; Zanasi, R. Induced Orbital Paramagnetism and Paratropism in Closed-Shell Molecules. *J. Phys. Chem. A* **2009**, *113*, 14465–14479.
- [28] Valiev, R. R.; Baryshnikov, G. V.; Nasibullin, R. T.; Sundholm, D.; Ågren, H. When Are Antiaromatic Molecules Paramagnetic? *J. Phys. Chem. C* **2020**, *124*, 21027–21035.
- [29] Valiev, R. R.; Fliegl, H.; Sundholm, D. Closed-shell paramagnetic porphyrinoids. *Chem. Comm.* **2017**, *53*, 9866–9869.
- [30] Peeks, M. D.; Claridge, T. D.; Anderson, H. L. Aromatic and antiaromatic ring currents in a molecular nanoring. *Nature* **2017**, *541*, 200–203.
- [31] Pascal, P. Recherches Magnetochimiques. *Ann. Chim. Phys.* **1910**, *19*, 5–70.

- [32] Coriani, S.; Lazzeretti, P.; Malagoli, M.; Zanasi, R. On CHF Calculations of 2nd-Order Magnetic Properties Using the Method of Continuous Transformation of Origin of the Current-Density. *Theor. Chim. Acta* **1994**, *89*, 181–192.
- [33] Zanasi, R.; Lazzeretti, P.; Malagoli, M.; Piccinini, F. Molecular magnetic properties within continuous transformations of origin of the current density. *J. Chem. Phys.* **1995**, *102*, 7150–7157.
- [34] Lazzeretti, P.; Malagoli, M.; Zanasi, R. Coupled Hartree–Fock calculations of origin-independent magnetic properties of benzene molecule. *J. Chem. Phys.* **1995**, *102*, 9619–9625.
- [35] Zanasi, R. Coupled Hartree-Fock calculations of molecular magnetic properties annihilating the transverse paramagnetic current density. *J. Chem. Phys.* **1996**, *105*, 1460–1469.
- [36] Ligabue, A.; Pincelli, U.; Lazzeretti, P.; Zanasi, R. Current Density Maps, Magnetizability, and Nuclear Magnetic Shielding Tensors for Anthracene, Phenanthrene, and Triphenylene. *J. Am. Chem. Soc.* **1999**, *121*, 5513–5518.
- [37] Lazzeretti, P. Methods of continuous translation of the origin of the current density revisited. *Theo. Chem. Acc.* **2012**, *131*, 1222–1234.
- [38] Lazzeretti, P. Erratum to: Methods of continuous translation of the origin of the current density revisited. *Theo. Chem. Acc.* **2012**, *132*, 1317–1317.
- [39] Steiner, E.; Fowler, P. W.; Havenith, R. W. A. Current Densities of Localized and Delocalized Electrons in Molecules. *J. Phys. Chem. A* **2002**, *106*, 7048–7056.
- [40] Soncini, A.; Teale, A. M.; Helgaker, T.; De Proft, F.; Tozer, D. J. Maps of current density using density-functional methods. *J. Chem. Phys.* **2008**, *129*, 074101:1–15.
- [41] London, F. Théorie quantique des courants interatomiques dans les combinaisons aromatiques. *J. Phys. Rad.* **1937**, *8*, 397–409.
- [42] Hameka, H. F. On the nuclear magnetic shielding in the hydrogen molecule. *Mol. Phys.* **1958**, *1*, 203–215.
- [43] Ditchfield, R. Self-consistent perturbation theory of diamagnetism. *Mol. Phys.* **1974**, *27*, 789–807.
- [44] Helgaker, T.; Jørgensen, P. An electronic Hamiltonian for origin independent calculations of magnetic properties. *J. Chem. Phys.* **1991**, *95*, 2595–2601.
- [45] Pedersen, T. B.; Koch, H.; Hättig, C. Gauge invariant coupled cluster response theory. *J. Chem. Phys.* **1999**, *110*, 8318–8327.
- [46] Jusélius, J.; Sundholm, D.; Gauss, J. Calculation of current densities using gauge-including atomic orbitals. *J. Chem. Phys.* **2004**, *121*, 3952–3963.
- [47] Taubert, S.; Sundholm, D.; Jusélius, J. Calculation of spin-current densities using gauge-including atomic orbitals. *J. Chem. Phys.* **2011**, *134*, 054123.

- [48] Fliegl, H.; Taubert, S.; Lehtonen, O.; Sundholm, D. The gauge including magnetically induced current method. *Phys. Chem. Chem. Phys.* **2011**, *13*, 20500–20518.
- [49] Sundholm, D.; Fliegl, H.; Berger, R. J. F. Calculations of magnetically induced current densities: theory and applications. *WIREs Comput. Mol. Sci.* **2016**, *6*, 639–678.
- [50] Taubert, S.; Kaila, V. R. I.; Sundholm, D. Aromatic pathways in conjugated rings connected by single bonds. *Int. J. Quantum Chem.* **2011**, *111*, 848–857.
- [51] Keith, T. A. Calculation of magnetizabilities using GIAO current density distributions. *Chem. Phys.* **1996**, *213*, 123 – 132.
- [52] Jusélius, J.; Sundholm, D.; co-workers, GIMIC, Gauge-Including Magnetically Induced Currents, a program for calculating of magnetically induced current density. Available from <https://github.com/qmcurrents/gimic/>.
- [53] Furche, F.; Ahlrichs, R.; Hättig, C.; Klopper, W.; Sierka, M.; Weigend, F. Turbomole. *WIREs Comput. Mol. Sci.* **2014**, *4*, 91–100.
- [54] Frisch, M. J.; *et al.*, Gaussian 16 Revision C.01. 2016; Gaussian Inc. Wallingford CT.
- [55] Dalton, a molecular electronic structure program, Release Dalton2016 (2015), see <http://daltonprogram.org..>
- [56] Stanton, J. F.; Gauss, J.; *et al.*, 2009; CFOUR, Coupled Cluster techniques for Computational Chemistry.
- [57] Reiter, K.; Weigend, F.; Wirz, L. N.; Dimitrova, M.; Sundholm, D. Magnetically Induced Current Densities in Toroidal Carbon Nanotubes. *J. Phys. Chem. C* **2019**, *123*, 15354–15365.
- [58] Pauling, L. The Diamagnetic Anisotropy of Aromatic Molecules. *J. Chem. Phys.* **1936**, *4*, 673–677.
- [59] Lonsdale, K. Magnetic Anisotropy and Electronic Structure of Aromatic Molecules. *Proc. R. Soc. (London) A* **1937**, *159*, 149–161.
- [60] Pople, J. Molecular orbital theory of aromatic ring currents. *Mol. Phys.* **1958**, *1*, 175–180.
- [61] McWeeny, R. Ring currents and proton magnetic resonance in aromatic molecules. *Mol. Phys.* **1958**, *1*, 311–321.
- [62] Fliegl, H.; Sundholm, D.; Taubert, S.; Jusélius, J.; Klopper, W. Magnetically Induced Current Densities in Aromatic, Antiaromatic, Homoaromatic, and Nonaromatic Hydrocarbons. *J. Phys. Chem. A* **2009**, *113*, 8668–8676.
- [63] Ahrens, J.; Geveci, B.; Law, C. ParaView: An End-User Tool for Large Data Visualization, Visualization Handbook, Elsevier, 2005, ISBN-13: 978-0123875822, see also: <http://www.paraview.org>.

- [64] Bartkowski, K.; Dimitrova, M.; Chmielewski, P. J.; Sundholm, D.; Pawlicki, M. Aromatic and Antiaromatic Pathways in Triphyrin(2.1.1) Annulated with Benzo[b]heterocycles. *Chem. Eur. J.* **2019**, *25*, 15477–15482.
- [65] Sundholm, D.; Berger, R. J. F.; Fliegl, H. Analysis of the magnetically induced current density of molecules consisting of annelated aromatic and antiaromatic hydrocarbon rings. *Phys. Chem. Chem. Phys.* **2016**, *18*, 15934–15942.
- [66] Kumar, C.; Fliegl, H.; Sundholm, D. Relation Between Ring Currents and Hydrogenation Enthalpies for Assessing the Degree of Aromaticity. *J. Phys. Chem. A* **2017**, *121*, 7282–7289.
- [67] Monaco, G.; Zanasi, R. Delocalization energy retrieved from the current density tensor. *Phys. Chem. Chem. Phys.* **2019**, *21*, 11564–11568.
- [68] Patra, S. G.; Mandal, N. Aromaticity of N-heterocyclic carbene and its analogues: Magnetically induced ring current perspective. *Int. J. Quant. Chem.* **2020**, *120*, e26152.
- [69] Pochan, J. M.; Flygare, W. H. Direct measurement of the magnetic susceptibility tensor elements in 1,3-cyclohexadiene and comparison with benzene and other small ring compounds. *J. Am. Chem. Soc.* **1969**, *91*, 5928–5929.
- [70] Gomes, J. A. N. F.; Mallion, R. B. Aromaticity and Ring Currents. *Chem. Rev.* **2001**, *101*, 1349–1384.
- [71] Hückel, E. Quantentheoretische Beiträge zum Benzolproblem. *Z. Phys.* **1931**, *70*, 204–286.
- [72] Hückel, E. Quantentheoretische Beiträge zum Problem der aromatischen und ungesättigten Verbindungen. III. *Z. Phys.* **1932**, *76*, 628–648.
- [73] Breslow, R. Aromatic Character. *Chem. Eng. News* **1965**, *43*, 90–100.
- [74] Breslow, R. Antiaromaticity. *Acc. Chem. Res.* **1973**, *6*, 393–398.
- [75] Baird, N. C. Quantum organic photochemistry. II. Resonance and aromaticity in the lowest  $^3\pi\pi^*$  state of cyclic hydrocarbons. *J. Am. Chem. Soc.* **1972**, *94*, 4941–4948.
- [76] Rosenberg, M.; Dahlstrand, C.; Kilså, K.; Ottosson, H. Excited State Aromaticity and Antiaromaticity: Opportunities for Photophysical and Photochemical Rationalizations. *Chem. Rev.* **2014**, *114*, 5379–5425.
- [77] Vijay, V.; Madhu, M.; Ramakrishnan, R.; Benny, A.; Hariharan, M. Through-space aromatic character in excimers. *Chem. Comm.* **2020**, *56*, 225–228.
- [78] Heilbronner, E. Hückel molecular orbitals of Möbius-type conformations of annulenes. *Tetrahedron Lett.* **1964**, *5*, 1923–1928.
- [79] Herges, R. Topology in Chemistry: Designing Möbius Molecules. *Chem. Rev.* **2006**, *106*, 4820–4842.

- [80] Rappaport, S. M.; Rzepa, H. S. Intrinsically Chiral Aromaticity. Rules Incorporating Linking Number, Twist, and Writhe for Higher-Twist Möbius Annulenes. *J. Am. Chem. Soc.* **2008**, *130*, 7613–7619.
- [81] Lazzeretti, P. Assessment of aromaticity via molecular response properties. *Phys. Chem. Chem. Phys.* **2004**, *6*, 217–223.
- [82] Fowler, P. W.; Steiner, E.; Acocella, A.; Jenneskens, L. W.; Havenith, R. W. A. Mapping the modification of ring currents induced by cyclopenta-fusion on a naphthalene core. *J. Chem. Soc., Perkin Trans. 2* **2001**, 1058–1065.
- [83] Fowler, P. W.; Havenith, R. W. A.; Jenneskens, L. W.; Soncini, A.; Steiner, E. Paratropic Delocalized Ring Currents in Flattened Cyclooctatetraene Systems with Bond Alternation. *Angew. Chem. Int. Ed.* **2002**, *41*, 1558–1560.
- [84] Soncini, A.; Havenith, R. W. A.; Fowler, P. W.; Jenneskens, L. W.; Steiner, E. Control of the Diatropic  $\pi$  Ring Current in Strained Benzenes: Effects of Annelation with Cyclopropa, Cyclobuta, and Cyclobutadieno Clamping Groups. *J. Org. Chem.* **2002**, *67*, 4753–4758.
- [85] Dimitrova, M.; Sundholm, D. The aromatic character of [10]annulenes and dicupra[10]annulenes from current density calculations. *Phys. Chem. Chem. Phys.* **2018**, *20*, 1337–1346.
- [86] Berger, R. J. F.; Viel, A. The symmetry principle of antiaromaticity. *Z. Naturforsch.* **2020**, *75*, 327–339.
- [87] Weigend, F.; Ahlrichs, R. Balanced basis sets of split valence, triple zeta valence and quadruple zeta valence quality for H to Rn: Design and assessment of accuracy. *Phys. Chem. Chem. Phys.* **2005**, *7*, 3297–3305.
- [88] Rappoport, D.; Furche, F. Property-optimized Gaussian basis sets for molecular response calculations. *J. Chem. Phys.* **2010**, *133*, 134105.
- [89] Kaipio, M.; Patzschke, M.; Fliegl, H.; Pichierri, F.; Sundholm, D. The effect of fluorine substitution on the aromaticity of polycyclic hydrocarbons. *J. Phys. Chem. A* **2012**, *116*, 10257–10268.
- [90] Clar, E. *The Aromatic Sextet*; Wiley: New York, 1972.
- [91] Balaban, A.; von Ragué Schleyer, P.; Rzepa, H. S. Crocker, Not Armit and Robinson, Begat the Six Aromatic Electrons. *Chem. Rev.* **2005**, *105*, 3436–3447.
- [92] Benkyi, I.; Staszewska-Krajewska, O.; Gryko, D. T.; Jaszuński, M.; Stanger, A.; Sundholm, D. Interplay of Aromaticity and Antiaromaticity in N-Doped Nanographenes. *J. Phys. Chem. A* **2020**, *124*, 695–703.
- [93] Soncini, A.; Steiner, E.; Fowler, P. W.; Havenith, R. W. A.; Jenneskens, L. W. Perimeter Effects on Ring Currents in Polycyclic Aromatic Hydrocarbons: Circumcoronene and Two Hexabenzocoronenes. *Chem. Eur. J.* **2003**, *9*, 2974–2981.

- [94] Mishra, S.; Krzeszewski, M.; Pignedoli, C. A.; Ruffieux, P.; Fasel, R.; Gryko, D. T. On-surface synthesis of a nitrogen-embedded buckybowl with inverse Stone–Thrower–Wales topology. *Nat. Commun.* **2018**, *9*, 1714.
- [95] Fliegl, H.; Sundholm, D. Aromatic Pathways of Porphins, Chlorins and Bacteriochlorins. *J. Org. Chem.* **2012**, *77*, 3408–3414.
- [96] Fliegl, H.; Valiev, R.; Pichierri, F.; Sundholm, D. *Chemical Modelling*; 2018; Vol. 14; Chapter 1: Theoretical studies as a tool for understanding the aromatic character of porphyrinoid compounds, pp 1–42.
- [97] Aihara, J.; Nakagami, Y.; Sekine, R.; Makino, M. Validity and Limitations of the Bridged Annulene Model for Porphyrins. *J. Phys. Chem. A* **2012**, *116*, 11718–11730.
- [98] Woodward, R. B. Totalsynthese des Chlorophylls. *Angew. Chemie* **1960**, *72*, 651–662.
- [99] Reddy, J. S.; Anand, V. G. Planar Meso Pentafluorophenyl Core Modified Isophlorins. *J. Am. Chem. Soc.* **2008**, *130*, 3718–3719.
- [100] Reddy, B. K.; Basavarajappa, A.; Ambhore, M. D.; Anand, V. G. Isophlorinoids: The Antiaromatic Congeners of Porphyrinoids. *Chem. Rev.* **2017**, *117*, 3420–3443.
- [101] Valiev, R. R.; Fliegl, H.; Sundholm, D. New insights into magnetically induced current pathways and optical properties of isophlorins. *J. Phys. Chem. A* **2013**, *117*, 9062–9068.
- [102] Tsuda, A.; Osuka, A. Fully Conjugated Porphyrin Tapes with Electronic Absorption Bands That Reach into Infrared. *Science* **2001**, *293*, 79–82.
- [103] Ikeda, T.; Aratani, N.; Osuka, A. Synthesis of Extremely  $\pi$ -Extended Porphyrin Tapes from Hybrid meso-meso Linked Porphyrin Arrays: An Approach Towards the Conjugation Length. *Chem. Asian J.* **2009**, *4*, 1248–1256.
- [104] Călugăreanu, G. Sur les classes d'isotopie des noeuds tridimensionnels et leurs invariants. *Czech. Math. J.* **1961**, *11*, 588–625.
- [105] Pohl, W. F. The Self-Linking Number of a Closed Space Curve. *Indiana Univ. Math. J.* **1968**, *17*, 975–985.
- [106] White, J. H. Self-Linking and Gauss-Integral in Higher Dimensions. *Am. J. Math.* **1969**, *91*, 693–728.
- [107] Fuller, F. B. The Writhing Number of a Space Curve. *Proc. Natl. Acad. Sci.* **1971**, *68*, 815–819.
- [108] Wirz, L. N.; Dimitrova, M.; Fliegl, H.; Sundholm, D. Magnetically Induced Ring-Current Strengths in Möbius Twisted Annulenes. *J. Phys. Chem. Lett.* **2018**, *9*, 1627–1632.
- [109] Ajami, D.; Oeckler, O.; Simon, A.; Herges, R. Synthesis of a Möbius aromatic hydrocarbon. *Nature* **2003**, *426*, 819–821.



- [110] Castro, C.; Chen, Z.; Wannere, C. S.; Jiao, H.; Karney, W. L.; Mauksch, M.; Puchta, R.; van Eikema Hommes, N. J. R.; von Ragué Schleyer, P. Investigation of a Putative Möbius Aromatic Hydrocarbon. The Effect of Benzannelation on Möbius  $[4n]$ Annulene Aromaticity. *J. Am. Chem. Soc.* **2005**, *127*, 2425–2432.
- [111] Taubert, S.; Sundholm, D.; Pichierri, F. Magnetically Induced Currents in Bianthraquinodimethane-Stabilized Möbius and Hückel  $[16]$ Annulenes. *J. Org. Chem.* **2009**, *74*, 6495–6502.
- [112] Higashino, T.; Lim, J.; Miura, T.; Saito, S.; Shin, J.-Y.; Kim, D.; Osuka, A. Möbius Antiaromatic Bisphosphorus Complexes of  $[30]$ Hexaphyrins. *Angew. Chem. Int. Ed.* **2010**, *49*, 4950–4954.
- [113] Shimizu, S.; Aratani, N.; Osuka, A. meso-Trifluoromethyl-Substituted Expanded Porphyrins. *Chem. Eur. J.* **2006**, *12*, 4909–4918.
- [114] Rzepa, H. S. Lemniscular Hexaphyrins as Examples of Aromatic and Antiaromatic Double-Twist Möbius Molecules. *Org. Lett.* **2008**, *10*, 949–952.
- [115] Fliegl, H.; Sundholm, D.; Taubert, S.; Pichierri, F. Aromatic Pathways in Twisted Hexaphyrins. *J. Phys. Chem. A* **2010**, *114*, 7153–7161.
- [116] Fliegl, H.; Sundholm, D.; Pichierri, F. Aromatic Pathways in Mono- and Bisphosphorous Singly Möbius Twisted  $[28]$  and  $[30]$ Hexaphyrins. *Phys. Chem. Chem. Phys.* **2011**, *13*, 20659–20665.
- [117] Kroto, H. W.; Heath, J. R.; O'Brien, S. C.; Curl, R. F.; Smalley, R. E.  $C_{60}$ : Buckminsterfullerene. *Nature* **1985**, *318*, 162–163.
- [118] Elser, V.; Haddon, R. C. Icosahedral  $C_{60}$  – an Aromatic Molecule with a Vanishingly Small Ring Current Magnetic-Susceptibility. *Nature* **1987**, *325*, 792–794.
- [119] Zanasi, R.; Fowler, P. Ring currents and magnetisability in  $C_{60}$ . *Chem. Phys. Lett.* **1995**, *238*, 270–280.
- [120] Johansson, M. P.; Jusélius, J.; Sundholm, D. Sphere Currents of Buckminsterfullerene. *Angew. Chem. Int. Ed.* **2005**, *44*, 1843–1846.
- [121] Chen, Z.; Wu, J. I.; Corminboeuf, C.; Bohmann, J.; Lu, X.; Hirsch, A.; von Ragué Schleyer, P. Is  $C_{60}$  buckminsterfullerene aromatic? *Phys. Chem. Chem. Phys.* **2012**, *14*, 14886–14891.
- [122] Muñoz-Castro, A. Axis-dependent magnetic behavior of  $C_{60}$  and  $C_{60}^{10+}$ . consequences of spherical aromatic character. *Chem. Comm.* **2015**, *51*, 10287–10290.
- [123] Hirsch, A.; Chen, Z.; Jiao, H. Spherical Aromaticity in  $I_h$  Symmetrical Fullerenes: The  $2(N+1)^2$  Rule. *Angew. Chem. Int. Ed.* **2000**, *39*, 3915–3917.
- [124] Bühl, M.; Hirsch, A. Spherical aromaticity of fullerenes. *Chem. Rev.* **2001**, *101*, 1153–1183.

- [125] Chen, Z.; King, R. B. Spherical Aromaticity: Recent Work on Fullerenes, Polyhedral Boranes, and Related Structures. *Chem. Rev.* **2005**, *105*, 3613–3642.
- [126] Reiher, M.; Hirsch, A. From Rare Gas Atoms to Fullerenes: Spherical Aromaticity Studied From the Point of View of Atomic Structure Theory. *Chem. Eur. J.* **2003**, *9*, 5442–5452.
- [127] Johansson, M. P.; Sundholm, D.; Vaara, J. Au<sub>32</sub>: A 24-carat golden fullerene. *Angew. Chem. Int. Ed.* **2004**, *43*, 2678–2681.
- [128] Sundholm, D. C<sub>72</sub>: Gaudiene a Hollow and Aromatic All-Carbon Molecule. *Phys. Chem. Chem. Phys.* **2013**, *15*, 9025–9028.
- [129] Sundholm, D.; Wirz, L. N.; Schwerdtfeger, P. Novel hollow all-carbon structures. *Nanoscale* **2015**, *7*, 15886–15894.
- [130] Rauhalahti, M.; Muñoz-Castro, A.; Sundholm, D. Magnetic response properties of gaudiene - a cavernous and aromatic carbocage. *Phys. Chem. Chem. Phys.* **2016**, *18*, 18880–18886.
- [131] Sarkar, A.; Kroto, H.; Endo, M. HEMI-toroidal networks in pyrolytic carbon nanotubes. *Carbon* **1995**, *33*, 51 – 55.
- [132] Endo, M.; Takeuchi, K.; Kobori, K.; Takahashi, K.; Kroto, H. W.; Sarkar, A. Pyrolytic carbon nanotubes from vapor-grown carbon fibers. *Carbon* **1995**, *33*, 873–881.
- [133] Terrones, M.; Hsu, W. K.; Hare, J. P.; Kroto, H. W.; Terrones, H.; Walton, D. R. M.; Klinowski, J.; Mackay, A. L. Graphitic structures: from planar to spheres, toroids and helices. *Phil. Trans. R. Soc. London A* **1996**, *354*, 2025–2054.
- [134] Liu, J.; Dai, H.; Hafner, J. H.; Colbert, D. T.; Smalley, R. E.; Jans, S. T.; Dekker, C. Fullerene ‘crop circles’. *Nature* **1997**, *385*, 780–781.
- [135] Martel, R.; Shea, H. R.; Avouris, P. Rings of single-walled carbon nanotubes. *Nature* **1999**, *398*, 299–299.
- [136] Zel’dovich, Y. B. Electromagnetic interaction with parity violation. *Sov. Phys. JETP* **1958**, *6*, 1148–1155, [*Zh. Eksp. Teor. Fiz.* **1957**, *33*, 1531–1533].
- [137] Ceulemans, A.; Chibotaru, L. F.; Fowler, P. W. Molecular Anapole Moments. *Phys. Rev. Lett.* **1998**, *80*, 1861–1864.
- [138] Gray, C. G.; Karl, G.; Novikov, V. A. Magnetic multipolar contact fields: The anapole and related moments. *Am. J. Phys.* **2010**, *78*, 936–948.
- [139] Pelloni, S.; Lazzeretti, P.; Monaco, G.; Zanasi, R. Magnetic-field induced electronic anapoles in small molecules. *Rend. Fis. Acc. Lincei* **2011**, *22*, 105–112.
- [140] Papasimakis, N.; Fedotov, V. A.; Marinov, K.; Zheludev, N. I. Gyrotropy of a Metamolecule: Wire on a Torus. *Phys. Rev. Lett.* **2009**, *103*, 093901.

- [141] Berger, R. J. F. Prediction of a Cyclic Helical Oligoacetylene Showing Anapolar Ring Currents in the Magnetic Field. *Z. Naturforsch. B* **2012**, *67*, 1127–1131.
- [142] Tellgren, E. I.; Fliegl, H. Non-perturbative treatment of molecules in linear magnetic fields: Calculation of anapole susceptibilities. *J. Chem. Phys.* **2013**, *139*, 164118.
- [143] Dunlap, B. I. Connecting carbon tubules. *Phys. Rev. B* **1992**, *46*, 1933–1936.
- [144] Fowler, P.; Steiner, E. Pseudo- $\pi$  currents: rapid and accurate visualisation of ring currents in conjugated hydrocarbons. *Chem. Phys. Lett.* **2002**, *364*, 259 – 266.
- [145] Hoffmann, R. The Many Guises of Aromaticity: Is hype debasing a core chemical concept? *Am. Sci.* **2015**, *103*, 18–22.
- [146] Li, X.; Kuznetsov, A. E.; Zhang, H. F.; Boldyrev, A. I.; Wang, L. S. All-metal aromaticity and antiaromaticity. *Science* **2001**, *291*, 859–861.
- [147] Kuznetsov, A. E.; Birch, K. A.; Boldyrev, A. I.; Li, X.; Zhai, H. J.; Wang, L. S. All-Metal Antiaromatic Molecule: Retangular  $\text{Al}_4^{4-}$  in the  $\text{Li}_3\text{Al}_4^-$  Anion. *Science* **2003**, *300*, 622–625.
- [148] Chen, Z.; Corminboeuf, C.; Heine, T.; Bohmann, J.; von Ragué Schleyer, P. Do all-metal antiaromatic clusters exist? *J. Am. Chem. Soc.* **2003**, *125*, 13930–13931.
- [149] Fowler, P.; Havenith, R.; Steiner, E. Unconventional ring currents in an all-metal aromatic,  $\text{Al}_4^{2-}$ . *Chem. Phys. Lett.* **2001**, *342*, 85–90.
- [150] Lin, Y. C.; Jusélius, J.; Sundholm, D.; Gauss, J. Magnetically induced current densities in  $\text{Al}_4^{2-}$  and  $\text{Al}_4^{4-}$  species studied at the coupled-cluster level. *J. Chem. Phys.* **2005**, *122*, 214308.
- [151] Becke, A. D. Density-functional thermochemistry. III. The role of exact exchange. *J. Chem. Phys.* **1993**, *98*, 5648–5652.
- [152] Lee, C.; Yang, W.; Parr, R. G. Development of the Colle-Salvetti correlation-energy formula into a functional of the electron density. *Phys. Rev. B* **1988**, *37*, 785–789.
- [153] Valiev, R. R.; Benkyi, I.; Konyshov, Y. V.; Fliegl, H.; Sundholm, D. Computational Studies of Aromatic and Photophysical Properties of Expanded Porphyrins. *J. Phys. Chem. A* **2018**, *122*, 4756–4767.
- [154] Szczepanik, D. W.; Solá, M.; Andrzejak, M.; Pawełek, B.; Dominikowska, J.; Kukułka, M.; Dyduch, K.; Krygowski, T. M.; Szatyłowicz, H. The role of the long-range exchange corrections in the description of electron delocalization in aromatic species. *J. Comp. Chem.* **2017**, *38*, 1640–1654.
- [155] Casademont-Reig, I.; Woller, T.; Contreras-García, J.; Alonso, M.; Torrent-Sucarrat, M.; Matito, E. New electron delocalization tools to describe the aromaticity in porphyrinoids. *Phys. Chem. Chem. Phys.* **2018**, *20*, 2787–2796.
- [156] Casademont-Reig, I.; Ramos-Cordoba, E.; Torrent-Sucarrat, M.; Matito, E. How do the Hückel and Baird Rules Fade away in Annulenes? *Molecules* **2020**, *25*, 711.